CAPITAL UNIVERSITY OF SCIENCE AND TECHNOLOGY, ISLAMABAD

Influence of Inclined Magnetic Field on Mixed Convective Nanofluid Flow Inside Porous Cavity

by

Qurat ul Ain Rubab

A thesis submitted in partial fulfillment for the degree of Master of Philosophy

in the

Faculty of Computing
Department of Mathematics

2020

This Thesis is Dedicated To

My Affectionate Parents

For making me what I am today

without whom none of my success would be possible

and

My Brothers

For their unconditional love, endless support and Encouragement

because their prayes, sympathies steer my way towards success.

CERTIFICATE OF APPROVAL

Influence of Inclined Magnetic Field on Mixed Convective Nanofluid Flow Inside Porous Cavity

by

Qurat ul Ain Rubab

(MMT163007)

THESIS EXAMINING COMMITTEE

S. No.	Examiner	Name	Organization
(a)	External Examiner	Dr. Muhammad Farooq Khan	RIU, Rawalpindi
(b)	Internal Examiner	Dr. Muhammad Sagheer	CUST, Islamabad
(c)	Supervisor	Dr. Shafqat Hussain	CUST, Islamabad

Supervisor Name
Dr. Shafqat Hussain
May, 2020

Dr. Muhammad Sagheer
Head
Dept. of Mathematics
May, 2020

Dr. Muhammad Abdul Qadir
Dean
Faculty of Computing
May, 2020

Author's Declaration

I, **Qurat ul Ain Rubab** hereby state that my M. Phil thesis titled "**Influence of Inclined Magnetic Field on Mixed Convective Nanofluid Flow Inside Porous Cavity**" is my own work and has not been submitted previously by me for taking any degree from Capital University of Science and Technology, Islamabad or anywhere else in the country/abroad.

At any time if my statement is found to be incorrect even after my graduation, the University has the right to withdraw my M. Phil Degree.

(Qurat ul Ain Rubab)

(MMT163007)

Plagiarism Undertaking

I solemnly declare that research work presented in this thesis titled "**Influence of Inclined Magnetic Field on Mixed Convective Nanofluid Flow Inside Porous Cavity**" is solely my research work with no significant contribution from any other person. Small contribution/help wherever taken has been dully acknowledged and that complete thesis has been written by me.

I understand the zero tolerance policy of the HEC and Capital University of Science and Technology towards plagiarism. Therefore, I as an author of the above titled thesis declare that no portion of my thesis has been plagiarized and any material used as reference is properly referred/cited.

I undertake that if I am found guilty of any formal plagiarism in the above titled thesis even after award of M. Phil Degree, the University reserves the right to withdraw/revoke my M. Phil degree and that HEC and the University have the right to publish my name on the HEC/University website on which names of students are placed who submitted plagiarized work.

(Qurat ul Ain Rubab)

(MMT163007)

Acknowledgements

First and Foremost, all praise and gratitude to **Allah**, the propitious, the benevolent, the most merciful, the greayest of all, for giving me determination and strength to do research. His continuous grace and mercy was with me throughout my life and ever more during the tenure of my research. Countless salutation be upon His last prophet **Hazrat Muhammad (Peace Be Upon Him)**, who bestowed us the perfect code of life.

The work presented in thesis was accomplished under the animate directions, observant pursuit, intellectual support and enlightened supervision of **Dr. Shafqat Hussain**. I am grateful to his ever inspiring guidance, keen interest, scholarly comments and constructive suggestions throughout my research work. Indeed, I am indebted to his valuable advices which always served as beacon of light to get me through all the difficulties of research work. I am also very thankful to my teachers; **Dr. Muhammad Sagheer**; Professor in Capital University of Science and Technology; **Dr. Muhammad Afzal**, Assistant professor and **Dr. Abdul Rehman Kashif**, Associate professor in Capital University of Science and Technology; for being a good mentor.

I am also thankful to my friends **Dania** and **Ayesha Majeed** not only for helping but also for keeping motivated and encouraging me throughout the work. Sincere thanks to my fellows for their assistance.

I have no words to acknowledge sacrifices, efforts, encouragement and firm dedication from my affectionate father throughout my academic career and life, who made me what I am today. I can't express my love for my caring mother, whose prayers always give me strength to hold on. Many thanks to my siblings who helped me to achieve success in every sphere of life progressively through their endless patience, support and encouragement.

Qurat ul Ain Rubab

(MMT163007)

Abstract

In this thesis, a computational analysis has been performed on mixed convection in a double lid driven cavity in the presence of porous medium. Effects of inclined magnetic field and volumetric heat generation or absorption are also studied. The fluid inside the cavity is a mixture of alumina-water nanofluid. The cavity consists of top and bottom adiabatic walls whereas two vertical walls are kept at different temperature T_h and T_c. The left wall is hot while the right wall is cold. The dimensionless governing equations are discretized by using Galerkin weighted residual finite element method. In particular, the biquadratic element space is utilized to discretize the velocity and temperature components while discontinuous linear element is utilized for pressure component. Picard iteration technique is applied to linearize the discrete non-linear algebraic system of equations and then Gauss elimination method is adopted to solve the associated linear subproblem. The computational study is illustrated and analyzed by means of isotherms, streamlines and some useful plots.

Contents

List of Figures

List of Tables

Abbreviations

avg	Average
2D	Two Dimensional
FEM	Finite Element Method
FVM	Finite Volume Method
GFEM	Galerkin Finite Element Method
LBM	Lattice Botlzmann Method
MHD	Magnetohydrodynamics
PDEs	Partial Differential Equations

Symbols

Re	Reynolds number, $\frac{U_0 L}{\nu_f}$
Ha	Hartmann number, $B_0 L\sqrt{\frac{\sigma_f}{\mu_f}}$
Gr	Grashof number, $\frac{g\beta\triangle T L^3}{\nu_f^2}$
Q_0	Dimensionless heat generation/absorption coefficient
Pr	Prandtl number, $\frac{\nu_f}{\alpha_f}$
Nu_L	Nusselt number (local)
Nu_{avg}	Nusselt number (average)
(X, Y)	Dimensionless space coordinates
(x, y)	Dimensional space coordinates
g	Gravitational acceleration ($m\ s^{-2}$)
Ri	Richardson number $\frac{Gr}{Re^2}$
U, V	Dimensionless velocity components
u, v	Dimensional velocity components
$\mathbf{F}$	Force
A	Cross-section area
C_p	Specific heat ($J\ Kg^{-1}\ K^{-1}$)
q	Dimensionless heat generation/absorption parameter
D	Diameter
p	Pressure ($N\ m^{-2}$)
P	Dimensionless pressure
T	Temperature (K)
T_c	Temperature of right cold wall (K)
T_h	Temperature of left hot wall (K)

Da	Darcy number $\left(\frac{K}{L^2}\right)$
K	Permeability of porous medium (m^2)
Greek symbols	
α	Thermal diffusivity $(m^2\ s^{-1})$
ϵ	Porosity of medium
β	Thermal expansion coefficients (K^{-1})
θ	Non-dimensional temperature $\frac{T-T_c}{T_h-T_c}$
ρ	Density $(Kg\ m^{-3})$
κ	Thermal conductivity $(Wm^{-1}\ K^{-1})$
ϕ	Volume fraction of nanoparticles
μ	Dynamic viscosity $(kg\ m^{-1}\ s^{-1})$
ν	Kinematic viscosity $(m^2\ s^{-1})$
σ	Electrical conductivity
γ	Inclination angle of magnetic field
Φ	Viscous dissipation
Subscripts	
c	Cold
h	Hot
f	Fluid
nf	Nanofluid
s	Nanoparticles

Chapter 1

Introduction

Lid driven cavity is a well known problem that has been investigated since last three decades. It is a classical problem of fluid mechanics and has considerable complexity. When temperature difference is applied to any side of cavity, mixed convection is seemed responsible for heat transport process inside the cavity. A mixed forced-natural convection inside the cavity under the influence of magnetic field has a special significance because of its frequent applications in different industrial process. Problems related to lid driven cavities are mainly divided into two categories which include cavities having one moving lid or either with double moving lids. Chaterjee [1] has discussed about the one sided moving lid enclosure. The motion of both vertical upward and downward lids has been considerd. Considerable differences were analyzed in the flow profiles and the thermal fields for these cases. The effect of lid movements with variations in Ra has been noticed on drag forces. The bulk flow temperature has opposite behaviour against magnetic field i.e., it is enhanced at low value of Ha with upward movements of lids.

Hussain et al. [2] explored the mixed convection energy inside cavity having heat sources along with vertical walls movement. The movement of flow was enhanced due to the buoyancy force. Nanoparticle volume fraction and Richardson numbers play an important role in heat transfer. Entropy generation of system and kinetic

energy of the flow has been enhanced with increasing Ri. Nusselt number is influenced by increasing in inclination angle for different heat sources. Kefayati [3] studied the natural convection in a cavity subjected to alumina-water nanofluid under the influence of magnetic field by using LBM. This study has concluded that the heat flow is reduced with a rise in Hartmann number. The rise in nanoparticle volume fractions enhanced the heat transfer and also influenced by variation in Rayleigh number.

We find the influence of magnetic field at high level in most of the industrial applications. Salem et al. [4] have analyzed the influence of moveable top wall's direction in a linearly heated cavity. The rate of heat transfer was reduced by increasing magnetic field for parameters such that Reynolds, Grashof and Hartmann numbers. Modal and Sibanda [5] investigated the natural convective flow inside an inclined enclosure under the influence of buoyancy ratio along varying magnetic field. The horizontal lower side of the cavity has been non-uniformly heated whereas the left up-right side was heated uniformly. The flow pattern was influenced by buoyancy ratio and magnetic field directions. The fluid flow was greatly influenced by the multiple eddies of counter clockwise rotation. Due to gradient of temperature, the fluid is derived by the buoyancy forces.

In the study of two-sided wall cavities, Eelshehbey and Ahmed [6] studied the effect of warmed vertical wall of a cavity on mixed convective flow of nanofluid in the presence of inclined magnetic field layouts. The nanofluid model distinctly assimilated the influence of thermophoresis and Brownian motion on fluid's flow. Increase in non-dimensional parameters, i.e., Richardson and Hartmann numbers have reduced the value of Nu_{avg}. The movement of upper horizontal lid facilitates the fluid flow for the highest values of buoyancy ratio. Oztop and Degtekin [7] explored the combined force-free convective flow in a moveable double lid-driven heated square cavity by using FVM. Sheikholeslami and Chamkha [8] examined the effects of convective thermal energy transportation and fluid flow of iron oxide-water nanofluid in a double lid driven enclosure under the influence of variable

magnetic field.

The entropy analysis on the electrical unsteady magnetohydrodynamics (MHD) nanofluid of heat transfer and natural convective flow over a permeable streatching sheet was revealed by Daniel et al. [9]. Sheikholeslami and Rokni [10] studied Buongiorno model for nanofluid flow to analyze the effects of magnetic field over a stretching plate. The velocity of nanofluid and forced convection were enhanced with the rise in melting parameter. The Nusselt number was decayed with augmented porosity and melting parameters.

Orazio et al. [11] explored the simulation for mixed convective nanofluid flow inside the rectangular shaped cavity by considering LBM. The heat transfer rate was enforced at the boundaries of the cavity. The rate of heat transfer increased with an increase in inclination angle, this impact is influenced by buoyancy forces for higher values of Richardson number. Salimefendigil and Chamkha [12] studied the magnetohydrodynamic (MHD) mixed convection with a triangular wave shaped bottom wall filled with a non-Newtonian fluid under the influence of inclined magnetic field. The shear thinning fluid was influenced by the natural convective flow. The rate of heat transfer reduces with an increasing values of Ri, and the augmentation is more effective for shear thickening fluid. Pseudoplastic fluid has shown a reduced average heat transfer for increasing Ha. The Nu_{avg} enhances by increasing the inclination angle of magnetic field. Karimipour et al. [13] depicts the forced convection of nanofluid magnetohydrodynamic (MHD) and thermal convection in a microchannel at different magnetic field angles. They analyzed slip velocity and temperature jump in the presence of magnetic field. The fluid flow is influenced by magnetic field. Moreover by using alumina-water nanofluid instead of silver-water nanofluid an amplified heat transport was observed at the low values of Reynolds numbers along the wall of microchannel.

Internal heat parameters occur in some engineering problems. Influence of uniform heat generation and magnetic field was numerically investigated by Selimefendigil and Oztop [14] to inspect the nanofluid natural convection in enclosure installed with different obstacles. The rise in the value of external Rayleigh number enhanced the local and averaged Nu. Local and average thermal energy transportation was reduced for rising Rayleigh number as well as magnetic field. Influence of magnetic field alignments and internal heat parameters on thermal mixed convection inside lid driven cavity was investigated by Chamkha [15]. Inside the cavity the flow behaviour and the heat transfer was influenced by the presence of magnetic field.

The concept of porous medium is utilized in different fields of engineering and applied science. Hussain et al. [16] investigated the entropy generation on mixed convection flow in an inclined channel with enclosure in porous medium. The fluid movement was subjected to the buoyancy forces due to shear forces and heated wall of cavity. They analyzed that the heat transfer was enhanced for high Darcy number and porosity parameters. An augmentation in Nu_{avg} is observed for higher values of inclination angle and porosity parameter. Varol et al. [17] studied temperature distributions in terms of heat convection for nanofluid flow inside a diagonally distributed cavity poured with porous medium. Heat transfer was reduced with the insertion of inclined plate in a cavity. The flow field was symmetric inside the cavity for all parameters.

1.1 Thesis Contribution

The foremost objective of this work is to analyze the impact of oriented magnetic field on mixed convective nanofluid flow inside the enclosure. Alumina-water nanofluid is filled inside the cavity system along porous medium. Volumetric heat generation or absorption parameters are reviewed here to inspect heat absorption and generation inside the enclosure. The dimensionless governing equations are solved by using GFEM. The system of dimensionless equations are discretized by

using Q_2/P_1^{disc} finite element pair. Different physical parameters are used to inspect flow behaviour. Results are potrayed in the form of streamline contours and isotherms curves.

1.2 Thesis Framework

This thesis is further comprised of four chapters.

Chapter 2 provides the fundamental concepts and governing laws which are used to analyze the modeled problems in the subsequent chapters.

Chapter 3 discusses the review study of Hussain et al. [2]. In this chapter, we investigate the steady mixed convection nanofluid and volumetric heat generation or absorption under the influence of inclined magnetic field. The finite element pair Q_2/P_1^{disc} is adopted to discretize the system of non-dimensional equations, then GFEM is utilized to solve the governing non-linear PDEs. Results are analyzed by using isotherms, streamlines and graphs.

Chapter 4 extends the work of Hussain et al. [2] with the idea of porous medium. The system of dimensionless equations are discretized by using biquadratic element Q_2 and P_1^{disc} linear element and the non-dimensional PDEs are solved by using GFEM. Isotherms, sreamlines and graphs are used to analyze the results.

Chapter 5 summarizes the overall analysis performed in the prersent work.

Chapter 2

Fundamental Concepts and Governing Equations

In this chapter, we will discuss about fundamental laws, definitions related to fluid dynamics and dimensionless parameters. There is also a brief discussion about the solution methodology, i.e., GFEM.

2.1 Fundamental Concepts

Definition 2.1.1. (Fluid) [18]
"A fluid is a substance that moves and deforms continuously as long as the shear stress applied. A solid can resist a shear stress by a static deflection but a fluid cannot."

Definition 2.1.2. (Fluid Mechanics) [19]
"Fluid mechanics is defined as the science that deals with the behaviour of fluids at rest or in motion, and the interaction of fluid with solids or other fluids at the boundaries."

Definition 2.1.3. (Fluid Statics) [18]
"It is the branch of fluid mechanics that deals with the study of fluid at rest."

Definition 2.1.4. (Fluid Dynamics) [18]

"It is the branch of fluid mechanics that deals with the study of fluid in motion."

Definition 2.1.5. (Pressure) [19]

"The amount of applied force '**F**' per unit area 'A' is called pressure." it's unit is Pascal. Mathematically, it can be written as

$$P = \frac{\mathbf{F}}{A}. \tag{2.1}$$

Definition 2.1.6. (Density) [19]

"Density is defined as mass per unit volume." Symbolically, it is represented as

$$\rho = \frac{m}{\mathbf{V}}, \tag{2.2}$$

where ρ, m and V are density, mass and volume, respectively.

Definition 2.1.7. (Viscosity) [20]

"Viscosity is defined as the property of a fluid which offers resistance to the movement of one layer of fluid over another adjacent layer of the fluid."

Definition 2.1.8. (Kinematic Viscosity) [21]

"The ratio of the viscosity μ and the density ρ is known as the kinematic viscosity." Kinematic viscosity is represented as

$$\nu = \frac{\mu}{\rho}. \tag{2.3}$$

Definition 2.1.9. (Dynamic Viscosity) [19]

"It is the internal resistance between fluid layers which is the tangential force per unit area. It is also called absolute viscosity."Mathematically, it can be expressed as

$$\tau = \mu \left(\frac{du}{dy} \right), \tag{2.4}$$

where μ is dynamic viscosity.

Definition 2.1.10. (Shear Stress) [19]

"The tangential component of a force acting on a surface per unit area is called

shear stress." Mathematically, it is represented by

$$\tau = \frac{\mathbf{F}}{A}. \tag{2.5}$$

In the above expression τ, $\mathbf{F}$, A are shear stress, applied force and cross-section area of the material respectively.

Definition 2.1.11. (Nanofluid) [22]
"Nanofluids are relatively new class of fluids which consist of a base fluid with nano-sized particles (1-100nm) suspended with in them. These particles, generally a metal or metal oxides, increase conduction and convection processes by allowing more heat to transfer."

Definition 2.1.12. (Magnetohydrodynamics)
"Magnetohydrodynamics is defined as the interaction of magnetic field and electrical conductance of liquids such as plasma, liquid metal and salt water etc."

Definition 2.1.13. (Magnetic Field)
"Magnetic field is the illustration of electric charges which are in relative motion and magnetized materials. Magnetic field is the main component of elecromagnetic force. Magnetic fields are used throughout modern technology, particularly in electrical engineering and electromechanics."

Definition 2.1.14. (Porous Medium) [23]
"A material consisting of a solid matrix with an interconnected void, is known as porous medium." Porous medium is subdivided into two types

1. Natural porous medium (sand stone, human lungs, wood, rye bread, etc.)
2. Man-made porous medium (ceramics, cements, cheese, sponges, etc.)

Definition 2.1.15. (Porosity) [23]
"The porosity of a porous medium is defined as the fraction of the total volume of the medium that is occupied by the void space." It can be expressed as

$$\epsilon = \frac{V_{void}}{V_{solid}},$$

where V_{solid} is the volume occupied by the solid particles and V_{void} is the volume occupied by the voids.

2.2 Classification of Fluid

Definition 2.2.1. (Ideal Fluid) [20]

"A fluid which is incompressible and has no viscosity, is known as an ideal fluid".

Definition 2.2.2. (Real Fluid) [20]

"A fluid, which possesses viscosity is known as real fluid. All the fluid in actual practice, are real fluids."

Definition 2.2.3. (Newtonian Fluid) [20]

"A real fluid, in which the shear stress is directly proportional to the rate of shear strain (or velocity gradient), is known as a Newtonian fluid". Most known Newtonian fluids are air, water, gasoline and oil etc.

Definition 2.2.4. (Non-Newtonian Fluid) [19]

"Fluids for which the shear stress is not linearly proportional to the shear strain rate are called non-Newtonian fluids". Most known non-Newtonian fluids are colloidal suspensions and slurries, polymer solutions, blood and paste etc.

2.3 Types of Flow

Definition 2.3.1. (Turbulent Flow) [24]

"Increase in speed may lead to instability that eventualy produces a more random type of flow, such flow is called turbulent flow."

Definition 2.3.2. (Laminar Flow) [19]

"Laminar fluid characterised by smooth streamlines and highly ordered motion."

Definition 2.3.3. (Steady Flow) [19]

"The term steady implies no change of properties, velocity, temperature, etc., at a

point with time. Many devices such as turbines, compressors, boilers, condensers, and heat exchangers operate for long period of time under the same conditions, and they are classified as steady flow devices."

Definition 2.3.4. (Unsteady Flow) [19]
"In fluid mechanics, unsteady is the most general term that applies to any flow that is not steady, but transient. The term periodic refers to the kind of unsteady flow in which the flow oscillates about a steady mean."

Definition 2.3.5. (Compressible Flow)
"The fluid in which the material density varies during fluid flow is said to be compressible flow." Compressible fluid flow is used in high speed jet engines, aircraft, rocket motors also in high speed usage in a planetary atmosphere etc.

Definition 2.3.6. (Incompressible Flow) [19]
"The flow is said to be incompressible if the density remains constant throughout."

Definition 2.3.7. (Uniform Flow)
"A flow is said to be uniform, when the velocity does not change in direction nor in magnitude at any point in a flowing fluid, for a given time."

Definition 2.3.8. (Non-Uniform Flow) [19]
"If the flow velocity varies with distance in the flow direction, then the flow is called non-uniform or varied flow."

Definition 2.3.9. (External Flow) [19]
"The flow of unbounded fluid over a surface such as a wire, a plate or a pipe is external flow. "

Definition 2.3.10. (Internal Flow) [19]
"The flow in a pipe or duct is internal flow if the fluid is completely bounded by a solid surfaces. Water flow in a pipe, for example, is internal flow."

2.4 Heat Transfer Mechanisms

Definition 2.4.1. (Conduction) [21]

"The transfer of heat from one part of a body at higher temperature to another part of the same body at lower temperature is called conduction. The conduction process takes place at molecular level and involves the transfer of energy from the more energetic molecules to those with a lower energy level." It is represented by

$$q^* = -kA\left(\frac{dT}{dx}\right). \tag{2.6}$$

In the above relation, k is the thermal conductivity.

Definition 2.4.2. (Convection) [21]

"Convection is the mode of heat transfer that relates to the transfer of heat from a bounding surface (container) to a fluid in motion. It is simply the flow of heat through fluids either liquids or gases."Mathematical expression for convection is

$$q^* = hA\left(T_w - T_\infty\right), \tag{2.7}$$

where q^*, h, T_w and T_∞ are heat transfer rate, heat transfer coefficient, surface temperature and temperature away from the surface, respectively.

Definition 2.4.3. (Forced Convection) [21]

"It is the type of convection in which some external source is used to induce a force on the fluid's system for the transportation of heat. External source may be a pump, fan, or some similar device."

Definition 2.4.4. (Natural Convection) [21]

"The heat transfer between a surface and fluid moving over it with the fluid motion caused entirely by the buoyancy forces that arises due to density changes that result from the temperature variations in the flow."

Definition 2.4.5. (Mixed Convection) [21]

"Mixed convection occurs when both natural convection and forced convection play significant roles in the transfer of heat."

Definition 2.4.6. (Thermal Conductivity) [18]

"The thermal conductivity is defined as a fluid property that varies with temperature and pressure in much the same way as viscosity. It is denoted by k. Fourier's law of conduction is related to the transfer of heat per unit area $\mathbf{q}''$, and the vector gradient of temperature ∇T."

$$\mathbf{q}'' = -k\nabla T,$$

where k, $\mathbf{q}''$ and ∇T are thermal conductivity, heat transfer and temperature gradient, repectively.

Definition 2.4.7. (Thermal Diffusivity) [21]

"Thermal diffusivity is defined as the ratio of thermal conductivity k, the density ρ, and the specific heat c_p at constant pressure. Heat transfer will occur whenever there exists a temperature difference in a medium." It can be represented by

$$\alpha = \frac{k}{\rho c_p}.$$

2.5 Non-dimensional Numbers

Definition 2.5.1. (Prandtl Number) [25]

"This number expresses the ratio of the momentum diffusivity (viscosity) to the thermal diffusivity. It characterizes the physical properties of a fluid with convective and diffusive heat transfers."Mathematically, it is expressed by

$$Pr = \frac{\text{viscous diffusion rate}}{\text{thermal diffusion rate}} = \frac{\nu}{\alpha} = \frac{c_p \mu}{k},$$

where ν and α are kinematic viscosity and thermal diffusivity, respectively.

Definition 2.5.2. (Grashof Number) [25]

"It expresses buoyancy to viscous forces ratio and its action on a fluid. It characterizes the free convection of fluid due to the density difference caused by the

temperature gradient in the fluid." It's mathematical form is

$$Gr = \frac{g\beta\Delta T L^3}{\nu^2}.$$

In above equation, β and ν are the coefficient of volumetric thermal expansion and viscosity.

Definition 2.5.3. (Reynolds number) [25]
"It is formulated as the ratio of the fluid inertia force to that of molecular friction (viscosity)".

$$Re = \frac{u_0 L}{\nu},$$

where L and u_0 are length scales of the flow and characteristic velocity and ν is the dynamic viscosity.

Definition 2.5.4. (Richardson Number) [25]
"This number expresses the ratio of the potential energy to the kinetic energy."

$$Ri = \frac{gh}{w^2} = \frac{Gr}{Re^2}.$$

Re and Gr are the Reynolds number and Grashof number, respectively.

Definition 2.5.5. (Hartmann Number) [25]
"It is a ratio of electromagnetic force to viscous force (molecular friction force)."

$$Ha = B_0 L \sqrt{\frac{\sigma_f}{\mu_f}},$$

where B_0, L, σ_f and μ_f are magnetic induction, characteristic length, electrical conductance and dynamic viscosity, respectively.

Definition 2.5.6. (Nusselt Number) [25]
"It expresses the ratio of total heat transfer in a system to the heat transfer by the conduction."

$$Nu_L = \frac{\text{convective heat transfer}}{\text{conductive heat transfer}} = \frac{hL}{k}.$$

h is convective heat transfer coefficient of fluid, k is thermal conductivity, L is characteristic length.

Definition 2.5.7. (Darcy Number) [25]
"It characterizes the permeability in porous material and in microchannels."It's mathematical form is

$$Da = \frac{K}{L^2},$$

where porous layer permeability is K and L is the thickness of porous layer.

2.6 Governing Equations

2.6.1 Continuity Equation

"The continuity equation describes the rate of change of density at a fixed point in the fluid."For a volume element fixed in space [21]

$$\frac{\partial \rho}{\partial t} + \nabla \cdot (\rho\ \mathbf{V}) = 0, \tag{2.8}$$

where, the velocity is represented by $\mathbf{V}$.
For steady case, equation of continuity becomes

$$\nabla \cdot (\rho \mathbf{V}) = 0. \tag{2.9}$$

For incompressible fluid the equation of continuity is

$$\nabla \cdot \mathbf{V} = 0. \tag{2.10}$$

2.6.2 Law of Conservation of Momentum

The momentum equation for a stationary volume element is as follow [21]

$$\frac{\partial \rho \mathbf{V}}{\partial t} + (\nabla \cdot \rho \mathbf{V})\, \mathbf{V} = -\nabla p + \nabla \cdot \mathbf{T} + \rho \mathbf{g}. \tag{2.11}$$

By using continuity equation, equation (2.11) is given as

$$\rho\left(\frac{\partial \mathbf{V}}{\partial t}+\mathbf{V}\cdot\nabla\mathbf{V}\right)=-\nabla p+\nabla\cdot\mathbf{T}+\rho\mathbf{g}. \tag{2.12}$$

In above equation, ρ is the density, p is the pressure, and $\mathbf{g}$ denotes the gravitational force.

For Navier Stokes equaion

$$\mathbf{T}=-p\mathbf{I}+\mu\tau', \tag{2.13}$$

τ' is the stress tensor

$$\tau'=\text{grad}\mathbf{V}+(\text{grad}\mathbf{V})^{*}, \tag{2.14}$$

where '$*$' is the transpose, the velocity field is $\mathbf{V}$.

The matrix form stress tensor τ' is expressed as

$$\tau'=\begin{pmatrix}\sigma_{xx} & \tau'_{yx} & \tau'_{zx}\\ \tau'_{xy} & \sigma_{yy} & \tau'_{zy}\\ \tau'_{xz} & \tau'_{yz} & \sigma_{zz}\end{pmatrix}. \tag{2.15}$$

The diagonal elements of Cauchy stress tensor σ_{yy}, σ_{xx}, and σ_{zz} are called normal stresses, and the rest are shear stresses.

We have velocity component $\mathbf{V}=[u(x,y,0),v(x,y,0),0]$ for 2D flow and thus

$$\text{grad}\mathbf{V}=\begin{pmatrix}\frac{\partial u}{\partial x} & \frac{\partial v}{\partial x} & 0\\ \frac{\partial u}{\partial y} & \frac{\partial v}{\partial y} & 0\\ 0 & 0 & 0\end{pmatrix}. \tag{2.16}$$

$$(\text{grad}\mathbf{V})^{*}=\begin{pmatrix}\frac{\partial u}{\partial x} & \frac{\partial u}{\partial y} & 0\\ \frac{\partial v}{\partial x} & \frac{\partial v}{\partial y} & 0\\ 0 & 0 & 0\end{pmatrix}. \tag{2.17}$$

Subsituting Eqs. (2.16) and (2.17) in Eq. (2.13) it is found that

$$\mathbf{T}_{xx} = -p + 2\mu\frac{\partial u}{\partial x} \tag{2.18}$$

$$\mathbf{T}_{xy} = \mu\left(\frac{\partial v}{\partial x} + \frac{\partial u}{\partial y}\right). \tag{2.19}$$

Using Eqs. (2.18) and (2.19) in Eq. (2.12) to obtain 2D Navier stokes equations for u-component

$$\rho\left(\frac{\partial u}{\partial t} + u\frac{\partial u}{\partial x} + v\frac{\partial u}{\partial y}\right) = -\frac{\partial p}{\partial x} + \mu\left(\frac{\partial^2 u}{\partial x^2} + \frac{\partial^2 u}{\partial y^2}\right) + \rho\ \mathbf{g}_{\ x}. \tag{2.20}$$

Similarly, for v-component, we obtain

$$\rho\left(\frac{\partial v}{\partial t} + u\frac{\partial v}{\partial x} + v\frac{\partial v}{\partial y}\right) = -\frac{\partial p}{\partial y} + \mu\left(\frac{\partial^2 v}{\partial x^2} + \frac{\partial^2 v}{\partial y^2}\right) + \rho\mathbf{g}_y. \tag{2.21}$$

2.6.3 Energy Equation

The energy equation in terms of first law of thermodynamics is expressed as [21]

$$\rho\frac{D\widehat{U}}{Dt} = -\nabla\cdot\mathbf{q}'' - p\,(\nabla\cdot\mathbf{V}) + \nabla\mathbf{V} : \tau + q''', \tag{2.22}$$

where heat flux is $\mathbf{q}''$, the internal heat generation is $\widehat{U}$, τ is the viscous force, $\nabla\mathbf{V} : \tau$ is a dissipation term and q''' is the rate of heat generation per unit volume. For a Newtonian fluid,

$$\nabla\mathbf{V} : \tau = \mu\Phi, \tag{2.23}$$

where Φ is the dissipation function.

By using Eq. (2.23) in Eq. (2.22), we get

$$\rho\frac{D\widehat{U}}{Dt} = -\nabla\cdot\mathbf{q}'' - p\,(\nabla\cdot\mathbf{V}) + \mu\Phi + q''', \tag{2.24}$$

where the rate of work done on fluid by pressure forces, i.e., $p\left(\nabla \cdot \mathbf{V}\right) = 0$ due to contribution of continuity equation, so

$$\rho\frac{\partial \widehat{U}}{\partial t} + \rho\mathbf{V} \cdot \left(\nabla \widehat{U}\right) = -\nabla \cdot \mathbf{q}'' - p\left(\nabla \cdot \mathbf{V}\right) + \mu\Phi + q'''. \tag{2.25}$$

Using definition of enthalpy into Eq. (2.25), it can be rearranged as

$$\widehat{U} = h - \frac{p}{\rho},$$

$$\rho\frac{\partial\left(h - \frac{p}{\rho}\right)}{\partial t} + \rho\mathbf{V} \cdot \left(\nabla\left(h - \frac{p}{\rho}\right)\right) = -\nabla \cdot \mathbf{q}'' - p\left(\nabla \cdot \mathbf{V}\right) + \mu\Phi + q''', \tag{2.26}$$

$$\rho\frac{\partial h}{\partial t} - \frac{\partial p}{\partial t} + \rho\mathbf{V} \cdot \left(\nabla h\right) - \mathbf{V} \cdot \left(\nabla p\right) = -\nabla \cdot \mathbf{q}'' - p\left(\nabla \cdot \mathbf{V}\right) + \mu\Phi + q'''. \tag{2.27}$$

After applying the Fourier's law (2.4), we get

$$\rho\frac{\partial h}{\partial t} - \frac{\partial p}{\partial t} + \rho\mathbf{V} \cdot \left(\nabla h\right) - \mathbf{V} \cdot \left(\nabla p\right) = -\nabla \cdot \left(-k\nabla T\right) - p\left(\nabla \cdot \mathbf{V}\right) + \mu\Phi + q''', \tag{2.28}$$

$$\rho\frac{\partial h}{\partial t} + \rho\mathbf{V} \cdot \left(\nabla h\right) = \frac{\partial p}{\partial t} + \mathbf{V} \cdot \left(\nabla p\right) + \nabla \cdot \left(k\nabla T\right) - p\left(\nabla \cdot \mathbf{V}\right) + \mu\Phi + q'''. \tag{2.29}$$

By using the physical relationship of enthalpy i.e., $dh = C_p dT$, then Eq. (2.29) becomes

$$\rho C_p\frac{\partial T}{\partial t} + \rho C_p\mathbf{V} \cdot \left(\nabla T\right) = \frac{\partial p}{\partial t} + \mathbf{V} \cdot \left(\nabla p\right) + \nabla \cdot \left(k\nabla T\right) - p\left(\nabla \cdot \mathbf{V}\right) + \mu\Phi + q''', \tag{2.30}$$

$$\rho C_p\frac{DT}{Dt} = \frac{Dp}{Dt} + \nabla \cdot \left(k\nabla T\right) - p\left(\nabla \cdot \mathbf{V}\right) + \mu\Phi + q'''. \tag{2.31}$$

For an incompressible, viscous and steady fluid, the energy equation becomes

$$\rho C_p \frac{DT}{Dt} = k\left(\nabla^2 T\right) + \mu\Phi + q'''. \tag{2.32}$$

2.7 Fundamentals of FEM

The FEM is a numerical technique which is applicable to all types of non-linear and linear partial differential equations. The whole domain is divided into small subdomains, usually triangular and quadrilateral in 2D. The solution on these subdomains is approximated using local nodal values. The approximate solution is obtained by using the Galerkin residual method. The partial differential equations are solved simulatneously, by matrix inversion or iteration method.

2.7.1 Galerkin Finite Element Method

The Galerkin weighted residual method is the class of methods for converting the continuous problems to discrete problems. Principally, it is equivalent to the method of variation of parameters to a function space, by transforming the equations to the weak formulations. It contains the following steps:

1. Discretize the whole computational domain $\Omega[c, d]$ of physical problem into number of small non-overlapping subintervals, i.e., $x_0 = c,\ x_1,\ x_2,\ \ldots,\ x_N = d$, where x_i is called a nodal points or nodes and $e_i = (x_i, x_{i+1})$ is an element. The mesh size for each domain is h_i such that $h_i = x_{i+1} - x_i$, for $i = 1, 2, \ldots, N-1$.

2. To obtain the variational form of the given strong form, first multiply the differential equation by weight function or test function $w \,\epsilon\, W$, where W is a test space. The test functions must satisfy the homogeneous Dirichlet boundary condition for Dirichlet boundary data. Then integrate by parts over the whole doamin.

3. Natural and essential boundary conditions are imposed on the boundary integrals and to the trial spaces, respectively.

4. Finite dimensional test space W_h and trial space U_h are utilized to approximate the infinite dimensional spaces where U_h (finite dimensional space) $\subset$ U (solution space) and $W_h \subset W$ (test space).

5. Galerkin discretization is applied to approximate finite dimensional trial solution and trial test spaces. Choose the approximate solution function u_h as $u_h \epsilon U_h$ such that $a(u_h, w_h) = b(w_h)$, for all $w_h \epsilon W$. Here $a(u_h, w_h)$ is known as the bilinear form while $b(w_h)$ notifies the linear form.

6. Represent the approximate solution over an element with finite dimensional trial solution space U_h by setting the linear combination of ϕ_j's with the nodal unknowns u_j's such that

$$u^e{}_j = \sum u^e{}_j \phi^e{}_j \quad j = 1, 2, \ldots, N. \tag{2.33}$$

   Similarly, for finite dimensional trial test space W_h

$$w^e{}_j = \sum w^e{}_i \phi^e{}_i \quad i = 1, 2, \ldots, N \tag{2.34}$$

7. Substituting approximate solution and test functions from Eqs. (2.33) and (2.34) into the variational formulation of the problem yields a linear elemental system of algebraic equations as given below

$$a\left(\sum u^e{}_j \phi^e{}_j, \phi^e{}_i\right) = b(\phi^e{}_i) \quad j, i = 1, 2, \ldots, N \tag{2.35}$$

$$\sum a\left(\phi^e{}_j, \phi^e{}_i\right) u^e{}_j = b(\phi^e{}_i) \quad j, i = 1, 2, \ldots, N \tag{2.36}$$

   where $u^e{}_j$ are the solution values at the respective nodal points of element e.

8. The above formulation will generate an algebraic linear system of equations, which contains equal number of equations as the number of elemental nodes

and will be written in the compact form as

$$[A^e]\{U^e\} = \{B^e\}. \tag{2.37}$$

9. To obtain following global system of equations, combine all local elemental system as in Eq. (2.37). The global system approximates the solution over the whole computational domain $\Omega = [c, d]$.

$$[A]\{U\} = \{B\}. \tag{2.38}$$

10. Finally, the approximate solution is obtained by solving the linear algebraic system of equation (2.38).

Chapter 3

Influence of Inclined Magnetic Field on Mixed Convective Nanofluid Flow

Influence of magnetic field on mixed convection is numerically investigated in this chapter. In order to solve the governing equations, we transform the system of dimensional equations into the dimensionless equations along with appropriate boundary conditions. To obtain the approximate solution of these equations GFEM is used. The results are presented in the form of graphs, isotherms and streamlines. In this chapter, the review of Hussain et al. [2] is provided.

3.1 Physical Model

Consider a laminar and steady nanofluid flow in a cavity with physical descriptions presented in Figure 3.1. It consists of double lid-driven cavity having horizontal upper and lower (adiabatic) sides with velocity u_0. The vertical walls of the cavity have different temperatures whereas right wall is maintained at temperature T_c and left one is at temperature T_h. Nanofluid is incompressible and Newtonian. Influence of radiations and slipping forces between any two phases are ignored.

Inclined magnetic field with an angle γ is applied. The heat dissipations due to magnetic and stresses are ignored. In buoyancy force, Boussinesq approximation approach is utilized to grasp density variation of nanofluid flow. Thermal properties of nanoparticles and base fluid are presented in Table 3.1. The effects of temperature on thermo-physical properties of nanoparticle and base fluid are ignored.

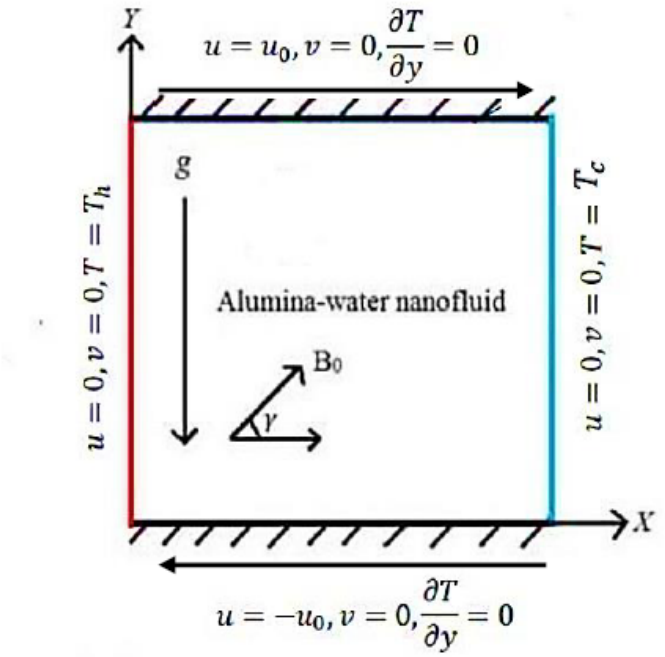

FIGURE 3.1: Configuration of phenomenal model.

TABLE 3.1: Thermo-physical properties of water and alumina. [16]

Physical Properties	**Water**	**Alumina**
ρ(Kg m^{-3})	$997 \cdot 1$	3970
c_p(JKg^{-1}K^{-1})	4179	765
k (Wm^{-1}K^{-1})	$0 \cdot 613$	40
β(K^{-1})	21×10^{-5}	$0 \cdot 85 \times 10{-}5$
$\sigma(\Omega\ \mathrm{m})^{-1}$	$0 \cdot 05$	1×10^{-10}
d_p(nm)	–	47

3.2 Dimensional Governing Equations

The governing equations of two-dimensional steady system with continuity, momentum and energy equations for an incompressible flow are given below [15, 26, 27]

- Continuity Equation:

$$\frac{\partial u}{\partial x}+\frac{\partial v}{\partial y}=0, \tag{3.1}$$

- x-Momentum Equation:

$$u\frac{\partial u}{\partial x}+v\frac{\partial u}{\partial y}=-\frac{1}{\rho_{nf}}\frac{\partial p}{\partial x}+\frac{\mu_{nf}}{\rho_{nf}}\left(\frac{\partial^2 u}{\partial x^2}+\frac{\partial^2 u}{\partial y^2}\right)+\frac{\sigma_{nf}B_0^2}{\rho_{nf}}(v\sin\gamma\cos\gamma-u\sin^2\gamma), \tag{3.2}$$

- y-Momentum Equation:

$$u\frac{\partial v}{\partial x}+v\frac{\partial v}{\partial y}=-\frac{1}{\rho_{nf}}\frac{\partial p}{\partial y}+\frac{\mu_{nf}}{\rho_{nf}}\left(\frac{\partial^2 v}{\partial x^2}+\frac{\partial^2 v}{\partial y^2}\right)+\frac{(\rho\beta)_{nf}}{\rho_{nf}}g(T-T_c)+\frac{\sigma_{nf}B_0^2}{\rho_{nf}}(u\sin\gamma\cos\gamma-v\cos^2\gamma), \tag{3.3}$$

- Energy Equation:

$$u\frac{\partial T}{\partial x}+v\frac{\partial T}{\partial y}=\alpha_{nf}\left(\frac{\partial^2 T}{\partial x^2}+\frac{\partial^2 T}{\partial y^2}\right)+\frac{Q_0}{(\rho C_p)_{nf}}(T-T_c). \tag{3.4}$$

The boundary conditions at different walls of the cavity corresponding to above dimensional equations from Eqs. (3.1) to (3.4) are written below:

- Upper horizontal side:

$$u=u_0,\quad v=0,\quad \frac{\partial T}{\partial y}=0.$$

- Lower horizontal side:

$$u = -u_0, \quad v = 0, \quad \frac{\partial T}{\partial y} = 0.$$

- Vertical left side:

$$u = 0, \quad v = 0, \quad T = T_h.$$

- Vertical right side:

$$u = 0, \quad v = 0, \quad T = T_c.$$

3.3 Physical Properties of Nanofluid

The relations for heat capacitance of nanofluid, electrical conductivity, thermal conductivity and effective density are given below [16, 26, 28]:

- Effective Density:

$$\rho_{nf} = \phi\rho_s + (1-\phi)\rho_f. \tag{3.5}$$

- Effective Thermal Diffusivity:

$$\alpha_{nf} = \frac{k_{nf}}{(\rho C_p)_{nf}}.$$

- Effective Electrical Conductivity:

$$\sigma_{nf} = \sigma_f \left[1 + \frac{3(\sigma-1)\phi}{(\sigma+2) - (\sigma-1)\phi}\right], \sigma = \frac{\sigma_s}{\sigma_f}.$$

- Effective Specific Heat:

$$(\rho C_p)_{nf} = \phi(\rho C_p)_s + (1-\phi)(\rho C_p)_f.$$

- Effective Coefficient of Thermal Expansion:

$$(\rho\beta)_{nf} = \phi(\rho\beta)_s + (1-\phi)(\rho\beta)_f. \tag{3.6}$$

Thermal conductivity of nanofluids is influenced by Bownian motion. A rule for effective thermal conductivity has been proposed by Koo and Kleinstreuer which is as follow [16, 29]

$$k_{eff} = k_{Brownian} + k_{static}, \tag{3.7}$$

$$k_{static} = k_f \left[1 + \frac{3\left(\frac{k_p}{k_f} - 1\right)\phi}{\left(\frac{k_p}{k_f} + 2\right) - \left(\frac{k_p}{k_f} - 1\right)\phi} \right]. \tag{3.8}$$

In the above equations, the thermal conductivity of solid particles, static and pure fluid are k_p , k_{static} and k_f respectively. It is based on Maxwell classical correlation. Koo-Kleinstreuer-Li proposed thermal conductivity in because of Brownian motion is given below

$$k_{Brownian} = 5 \times 10^4 \rho_f (C_p)_f \phi \sqrt{\frac{K_b T}{\rho_p d_p}} f'(T_{ref}, \phi, d_p), \tag{3.9}$$

where the value of f' is obtained from the following relation

$$\begin{aligned} f'(T_{ref}, \phi, d_p) = &\left[c_1 + c_2 \ln(d_p) + c_3 \ln(\phi) c_4 \ln(\phi) \ln(d_p) + c_5 \ln(d_p)^2\right] \ln(T_{ref}) \\ &+ \left[c_6 + c_7 \ln(d_p) + c_8 \ln(\phi) + c_9 \ln(d_p) \ln(\phi) + c_{10} \ln(d_p)^2\right], \end{aligned} \tag{3.10}$$

with the cefficients $c_i (i = 1, 2, \ldots, 10)$ as organized in Table 3.3. Moreover, Koo-Kleinstreuer introduced the effective viscosity model as follow

$$\mu_{eff} = \mu_{static} + \mu_{Brownian} = \mu_{static} + \frac{k_{Brownian}}{k_f} \times \frac{\mu_f}{P_{rf}}. \tag{3.11}$$

Brinkman proposed a model for nanofluids viscosity as given by

$$\mu_{static} = \mu_{nf} = \mu_f / (1 - \phi)^{2.5}. \tag{3.12}$$

Interfacial thermal resistance, i.e $R_f = 4 \times 10^{-8} K m^2/W$ and k_p in Eq. (3.8) is replaced by $k_{p,eff}$, which is obtained from the following relation

$$R_f + \frac{d_p}{k_p} = \frac{d_p}{k_{p,eff}}. \tag{3.13}$$

TABLE 3.2: The coefficients values of nanofluid.

Coefficients	**values**
c_1	$52 \cdot 813488759$
c_2	$6 \cdot 115637295$
c_3	$0 \cdot 6955745084$
c_4	$0 \cdot 041745555278$
c_5	$0 \cdot 176919300241$
c_6	$-298 \cdot 19819084$
c_7	$-34 \cdot 532716906$
c_8	$-3 \cdot 9225289283$
c_9	$-0 \cdot 2354329626$
c_{10}	$-0 \cdot 999063481$

3.3.1 Non-dimensional Governing Equations

The governing equations are transformed into dimensionless form by utilizing non-dimensional parameters, which are expressed as below

$$U = \frac{u}{u_0}, \quad \theta = \frac{T - T_c}{T_h - T_c}, \quad X = \frac{x}{L}, \quad V = \frac{v}{u_0}, \quad Y = \frac{y}{L}, \quad P = \frac{p}{\rho_{nf} u_0^2},$$

$$Re = \frac{u_0 L}{\nu_f}, \quad Gr = \frac{g\beta_f \triangle T L^3}{\nu_f^2}, \quad Pr = \frac{\nu_f}{\alpha_f}, \quad Ha = B_0 L \sqrt{\frac{\sigma_f}{\mu_f}}, \quad q = \frac{Q_0 L^2}{(\rho C_p)_{nf} \alpha_f}.$$

By using the dimesionless parametres, the governing system of equations becomes:

- Continuity Equation:

$$\frac{\partial U}{\partial X} + \frac{\partial V}{\partial Y} = 0 \tag{3.14}$$

- x-Momentum Equation:

$$U\frac{\partial U}{\partial X}+V\frac{\partial U}{\partial Y}=-\frac{\partial P}{\partial X}+\frac{1}{Re}\frac{\rho_f}{\rho_{nf}}\frac{1}{(1-\phi)^{2.5}}\left(\frac{\partial^2 U}{\partial X^2}+\frac{\partial^2 U}{\partial Y^2}\right)+\frac{\sigma_{nf}}{\sigma_f}\frac{\rho_f}{\rho_{nf}}\frac{Ha^2}{Re}(V\sin\gamma\cos\gamma-U\sin^2\gamma) \tag{3.15}$$

- y-Momentum Equation:

$$U\frac{\partial V}{\partial X}+V\frac{\partial V}{\partial Y}=-\frac{\partial P}{\partial Y}+\frac{1}{Re}\frac{\rho_f}{\rho_{nf}}\frac{1}{(1-\phi)^{2.5}}\left(\frac{\partial^2 V}{\partial X^2}+\frac{\partial^2 V}{\partial Y^2}\right)+\frac{\sigma_{nf}}{\sigma_f}\frac{\rho_f}{\rho_{nf}}\frac{Ha^2}{Re}(U\sin\gamma\cos\gamma-V\cos^2\gamma)+Ri\frac{\rho_f}{\rho_{nf}}\left(1-\phi+\frac{\rho_s\beta_s}{\rho_f\beta_f}\phi\right)\theta \tag{3.16}$$

- Energy Equation:

$$U\frac{\partial \theta}{\partial X}+V\frac{\partial \theta}{\partial Y}=\frac{\alpha_{nf}}{\alpha_f}\frac{1}{RePr}\left(\frac{\partial^2 \theta}{\partial X^2}+\frac{\partial^2 \theta}{\partial Y^2}\right)+\frac{1}{RePr}q\theta \tag{3.17}$$

The corresponding boundary conditions related to the above PDEs (3.14) to (3.17) are given below:

- Upper horizontal side:

$$V=0,\quad U=1,\quad \frac{\partial \theta}{\partial y}=0.$$

- Lower horizontal side:

$$V=0,\quad U=-1,\quad \frac{\partial \theta}{\partial y}=0.$$

- Vertical left side:

$$V=0,\quad U=0,\quad \theta=1.$$

- Vertical right side:

$$V=0,\quad U=0,\quad \theta=0.$$

Following expressions are used to estimate local and average Nusselt numbers

$$Nu = -\frac{k_{nf}}{k_f}\left|\left(\frac{\partial\theta}{\partial X}\right)\right|_{X=0},$$

$$Nu_{avg} = \int_0^1 Nu dY.$$

3.4 Numerical Solutions and Validations

The numerical solution of non-dimensional governing equations from (3.14) to (3.17) along the corresponding boundary conditions has been obtained by utilizing Galerkin weighted residual method. Governing system is discretized by using $Q_2/{P_1}^{disc}$ finite element pair in space, temperature and velocity-components (U, V) in Q_2 space and the term pressure is in ${P_1}^{disc}$ space. Firstly, we obtain the weak formulation of non-linear governing equations, then the approximate solution by using Galerkin residual method.

3.4.1 Variational / Weak Formulation

In variational formulation, the non-dimensional governing equations are converted into weak form, by multiplying the equations with functions of test spaces $\mathbf{W}$ and Q, then integrated over the whole domain Ω.

Let $\mathbf{W} = [H_1(\Omega)]^3$ and $Q = L_2(\Omega)$ be the test spaces for temperature, velocity components and pressure, respectively. The non-dimensional equations are as follow

$$\frac{\partial U}{\partial X} + \frac{\partial V}{\partial Y} = 0, \tag{3.18}$$

$$\left(U\frac{\partial U}{\partial X} + V\frac{\partial U}{\partial Y}\right) = -\frac{\partial P}{\partial X} + A_1\left(\frac{\partial^2 U}{\partial X^2} + \frac{\partial^2 U}{\partial Y^2}\right) + A_2(V\sin\gamma\cos\gamma - U\sin^2\gamma), \tag{3.19}$$

$$\left(U\frac{\partial V}{\partial X}+V\frac{\partial V}{\partial Y}\right)=-\frac{\partial P}{\partial Y}+A_1\left(\frac{\partial^2 V}{\partial X^2}+\frac{\partial^2 V}{\partial Y^2}\right)+A_3\theta + A_2\left(U\sin\gamma\cos\gamma-V\cos^2\gamma\right), \tag{3.20}$$

$$U\frac{\partial \theta}{\partial X}+V\frac{\partial \theta}{\partial Y}=A_4\left(\frac{\partial^2 \theta}{\partial X^2}+\frac{\partial^2 \theta}{\partial Y^2}\right)+A_5\theta. \tag{3.21}$$

In the above equations A_i's are given below

$$A_1=\frac{\rho_f}{\rho_{nf}}\frac{1}{Re}\frac{1}{(1-\phi)^{2.5}},\quad A_5=\frac{1}{RePr}q,\quad A_3=Ri\frac{\rho_f}{\rho_{nf}}\left(1-\phi+\frac{\rho_s\beta_s}{\rho_f\beta_f}\phi\right),$$
$$A_4=\frac{\alpha_{nf}}{\alpha_f}\frac{1}{RePr},\quad A_2=\frac{\rho_f}{\rho_{nf}}\frac{\sigma_{nf}}{\sigma_f}\frac{Ha^2}{Re}.$$

For weak formulation multiply the Eqs. (3.18) to (3.21) by test spaces $\mathbf{W}$ and Q, where $w\,\epsilon\,\mathbf{W}$ and $q\,\epsilon\,Q$ and then integrate over the whole domain Ω.

Find $(U,V,\theta,P)\ \epsilon\ \mathbf{W}\times Q$ such that

$$\int_\Omega\left(U\frac{\partial U}{\partial X}+V\frac{\partial U}{\partial Y}\right)wd\Omega+\int_\Omega\frac{\partial P}{\partial X}wd\Omega-A_1\int_\Omega\left(\frac{\partial^2 U}{\partial X^2}+\frac{\partial^2 U}{\partial Y^2}\right)wd\Omega - A_2\int_\Omega(V\sin\gamma\cos\gamma-U\sin^2\gamma)wd\Omega=0, \tag{3.22}$$

$$\int_\Omega\left(U\frac{\partial V}{\partial X}+V\frac{\partial V}{\partial Y}\right)wd\Omega+\int_\Omega\frac{\partial P}{\partial Y}wd\Omega-A_1\int_\Omega\left(\frac{\partial^2 V}{\partial X^2}+\frac{\partial^2 V}{\partial Y^2}\right)wd\Omega - A_3\int_\Omega\theta wd\Omega-A_2\int_\Omega(U\sin\gamma\cos\gamma-V\cos^2\gamma)wd\Omega=0, \tag{3.23}$$

$$\int_\Omega\frac{\partial U}{\partial X}qd\Omega+\int_\Omega\frac{\partial V}{\partial Y}qd\Omega=0, \tag{3.24}$$

$$\int_\Omega\left(U\frac{\partial \theta}{\partial X}+V\frac{\partial \theta}{\partial Y}\right)wd\Omega-A_4\int_\Omega\left(\frac{\partial^2\theta}{\partial X^2}+\frac{\partial^2\theta}{\partial Y^2}\right)wd\Omega-A_5\int_\Omega\theta wd\Omega=0, \tag{3.25}$$

for all $(w,q)\ \epsilon\ \mathbf{W}\times Q$.

Let $q\approx q_h,\quad V\approx V_h,\quad w\approx w_h,\quad \theta\approx\theta_h,\quad U\approx U_h,\quad P\approx P_h.$

By Galerkin's approximation method

$$\int_\Omega\frac{\partial U_h}{\partial X}q_hd\Omega+\int_\Omega\frac{\partial V_h}{\partial Y}q_hd\Omega=0, \tag{3.26}$$

$$A_1\int_\Omega\left(\frac{\partial U_h}{\partial X}\frac{\partial w_h}{\partial X}+\frac{\partial U_h}{\partial Y}\frac{\partial w_h}{\partial Y}\right)d\Omega+\int_\Omega\left(U_h\frac{\partial U_h}{\partial X}+V_h\frac{\partial U_h}{\partial Y}\right)w_h d\Omega$$
$$-\int_\Omega\frac{\partial w_h}{\partial X}P_h d\Omega+\omega_1\int_\Omega U_h w_h d\Omega-\omega_2\int_\Omega V_h w_h d\Omega=0, \tag{3.27}$$

$$A_1\int_\Omega\left(\frac{\partial V_h}{\partial X}\frac{\partial w_h}{\partial X}+\frac{\partial V_h}{\partial Y}\frac{\partial w_h}{\partial Y}\right)d\Omega+\int_\Omega\left(U_h\frac{\partial V_h}{\partial X}+V_h\frac{\partial V_h}{\partial Y}\right)w_h d\Omega$$
$$-\int_\Omega\frac{\partial w_h}{\partial Y}P_h d\Omega-\omega_2\int_\Omega U_h w_h d\Omega+\omega_3\int_\Omega V_h w_h d\Omega-A_3\int_\Omega\theta_h w_h d\Omega=0, \tag{3.28}$$

$$\int_\Omega\left(U_h\frac{\partial\theta_h}{\partial X}+V_h\frac{\partial\theta_h}{\partial Y}\right)w_h d\Omega+A_4\int_\Omega\left(\frac{\partial\theta_h}{\partial X}\frac{\partial w_h}{\partial X}+\frac{\partial\theta_h}{\partial Y}\frac{\partial w_h}{\partial Y}\right)d\Omega$$
$$-A_5\int_\Omega\theta_h w_h d\Omega=0. \tag{3.29}$$

In the above equations, ω_i's are represented as

$$\omega_1=A_2\sin^2\gamma,\qquad \omega_2=A_2\sin\gamma\cos\gamma,\qquad \omega_3=A_2\cos^2\gamma.$$

The FEM approximation functions for trial spaces and test spaces are given below

$$U_h=\sum_{j=1}^{n}U_jS_j,\quad V_h=\sum_{j=1}^{n}V_jS_j,\quad P_h=\sum_{j=1}^{m}P_j\eta_j,\quad \theta_h=\sum_{j=1}^{n}\theta_jS_j$$
$$w_h=\sum_{i=1}^{n}w_iS_i,\quad q_h=\sum_{i=1}^{m}q_i\eta_i.$$

Now inserting the approximate functions of test and trial spaces in equations (3.27) to (3.29), the matrix form of discretized system is

$$\begin{pmatrix}K^{11}&K^{12}&K^{13}&K^{14}\\K^{21}&K^{22}&K^{23}&K^{24}\\K^{31}&K^{32}&K^{33}&K^{34}\\K^{41}&K^{42}&K^{43}&K^{44}\end{pmatrix}\begin{pmatrix}\underline{U}\\\underline{V}\\\underline{P}\\\underline{\theta}\end{pmatrix}=\begin{pmatrix}\underline{F^1}\\\underline{F^2}\\\underline{F^3}\\\underline{F^4}\end{pmatrix}, \tag{3.30}$$

where $\underline{\theta}=\theta_j,\underline{V}=V_j,\underline{U}=U_j;\ j=1,2,\ldots,n$, and $\underline{P}=P_j;\ j=1,2,\ldots,m$. The vectors $\underline{F^1},\ldots,\underline{F^4}$ represent the corresponding R.H.S. The corresponding block

matrices are

$$K^{11}{}_{ij} = \int_\Omega \left(\sum_{j=1}^{n} U_j S_j \frac{\partial S_j}{\partial X} + \sum_{j=1}^{n} V_j S_j \frac{\partial S_j}{\partial Y} \right) S_i d\Omega + A_1 \int_\Omega \left(\frac{\partial S_j}{\partial X}\frac{\partial S_i}{\partial X} + \frac{\partial S_j}{\partial Y}\frac{\partial S_i}{\partial Y} \right) d\Omega + \omega_1 \int_\Omega S_j S_i d\Omega,$$

$$K^{22}{}_{ij} = \int_\Omega \left(\sum_{j=1}^{n} U_j S_j \frac{\partial S_j}{\partial X} + \sum_{j=1}^{n} V_j S_j \frac{\partial S_j}{\partial Y} \right) S_i d\Omega + A_1 \int_\Omega \left(\frac{\partial S_j}{\partial X}\frac{\partial S_i}{\partial X} + \frac{\partial S_j}{\partial Y}\frac{\partial S_i}{\partial Y} \right) d\Omega + \omega_3 \int_\Omega S_j S_i d\Omega,$$

$$K^{44}{}_{ij} = \int_\Omega \left(\sum_{j=1}^{n} U_j S_j \frac{\partial S_j}{\partial X} + \sum_{j=1}^{n} V_j S_j \frac{\partial S_j}{\partial Y} \right) S_i d\Omega + A_4 \int_\Omega \left(\frac{\partial S_j}{\partial X}\frac{\partial S_i}{\partial X} + \frac{\partial S_j}{\partial Y}\frac{\partial S_i}{\partial Y} \right) d\Omega - A_5 \int_\Omega S_j S_i d\Omega,$$

$$K^{12}{}_{ij} = -\omega_2 \int_\Omega S_j S_i d\Omega = K^{21}{}_{ij}, \quad K^{13}{}_{ij} = -\int_\Omega \frac{\partial S_i}{\partial X}\eta_j d\Omega, \quad K^{23}{}_{ij} = -\int_\Omega \frac{\partial S_i}{\partial Y}\eta_j d\Omega$$

$$K^{24}{}_{ij} = -A_3 \int_\Omega S_j S_i d\Omega, \quad K^{31}{}_{ij} = \int_\Omega \frac{\partial S_j}{\partial X}\eta_i d\Omega, \quad K^{32}{}_{ij} = \int_\Omega \frac{\partial S_j}{\partial Y}\eta_i d\Omega$$

$$K^{14}{}_{ij} = K^{33}{}_{ij} = K^{34}{}_{ij} = K^{41}{}_{ij} = K^{42}{}_{ij} = K^{43}{}_{ij} = 0.$$

Picard method is applied to linearize the system of non-linear equations. Gauss elimination method is used to solve the linearized system of equations. The stopping criterion for the convergence of system is mentioned below

$$\left| \frac{\Pi^{n+1} - \Pi^n}{\Pi^{n+1}} \right| \leqslant 10^{-6}$$

where Π indicates the dependent factors V, θ, P or U . Here, iteration number is represented by the superscript n in above expression.

3.4.2 Grid Generation and Refinement

First, at level $l = 1$, the coarsest grid containing one element is designed. Then the refined form of grid is obtained by dividing each element in further four new

elements in the way that the corresponding midpoints are joined for level $l = l+1$.

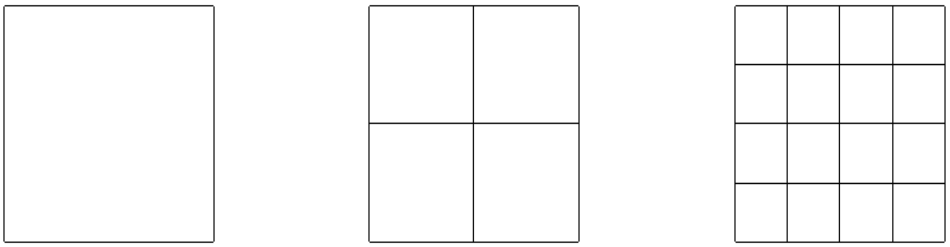

FIGURE 3.2: Spatial grid design for mesh $l = 1, 2, 3$ (from left to right).

3.4.3 Code Validations

In order to validate the code adopted for the numerical solution of mixed convection flow, the current results are compared with the previous results based on mixed convection flow. In Table 3.3, it is shown that the results are in good agreement as compared to the published results in literature.

TABLE 3.3: Comparison of present work with the some published results for $Gr = 100$. [2, 30–32]

Re	Present study [2]	Ref. [30]	Ref. [31]	Ref. [32]
100	2.03	-	2.05	1.94
400	4.07	4.08	4.09	3.84
1000	6.58	6.48	6.70	6.33

3.4.4 Grid Independent Test

The Nusselt number is computed for $q = 5$, $\phi = 0.04$, $Ha = 25$, $Ri = 5$, $\gamma = 0°$ and $Re = 100$ at different mesh level (l) along total degree of freedom (DOF) and number of elements (EL). The grid convergence test for different mesh levels is given in Table 3.4.

TABLE 3.4: Grid independence results for alumina-water nanofluid at $Ri = 1$.

l	EL	DOFs	Nu_{avg}
4	64	1059	$7 \cdot 176050$
5	256	4035	$7 \cdot 621126$
6	1024	15747	$7 \cdot 454072$
7	4096	62211	$7 \cdot 051243$
8	16384	247299	$6 \cdot 659882$

3.5 Results and Analysis

The impacts of magnetic field layouts on alumina-water mixed convective flow inside square cavity has been studied numerically. Figure 3.3 depicts the role of Ha on flow domain for $\gamma = 0°$, $q = 5$, $\phi = 0.04$, $Ri = 5$ and $Re = 100$. It is clear from the figure that both horizontal upper and lower sides move in opposite way. At $Ha = 0$, flow is concentrated about horizontal upper and lower sides due to high value of kinetic energy. Augmentation in magnetic force is reducing the thickness of cells. Reduction in kinetic energy of flow is noticed due to high strength of magnetic force. A visible and fine heat layers are distinctly seen with the left vertical wall at highest values of Ha. Due to high value of Hartmann number, heat generation is occured inside the enclosure. It is more prominent at high value of Hartmann number i.e., $Ha = 100$.

Influence of inclined magnetic field on streamlines and isotherms with $Ri = 5$, $Ha = 25$, $\phi = 0.04$, $Re = 100$ and $q = 5$ are displayed in Figure 3.4. It shown in figure, that inclined magnetic field has efficient effects on the thermal distribution and flow field. This impact seems more visible at $\gamma > 30°$. An increase in magnetic field inclination is main cause of increment in the flow movement. Here the influence of magnetic field is directly associated with kinetic energy.

Figure 3.5 illustrates the influence of Richardson number Ri on isotherms and streamlines with $\phi = 0.04, q = 5, Re = 100, \gamma = 0°$ and $Ha = 25$. At the low

value of Ri, high heat generation is occured. It reduces with an increase in Ri. The natural to forced convection dominates for increasing Ri. The position of cells is also changed with the variations of Ri. The flow movement also increases from vertical left to right wall of the cavity for high Richardson number. The effects of nanoparticles volume fraction are presented in Figure 3.6 with the help of isotherms and streamlines. The impact of nanoparticle volume fraction on thermal distribution and streamlines are not clear. Few variations have been noticed near the top and bottom lids of cavity.

The impact of volumetric heat parameters on isotherms and streamlines is shown in Figure 3.7 for parameters of $\gamma = 0°, Ha = 25, \phi = 0.04, Ri = 5$ and $Re = 100$. Temperature distribution is influenced by volumetric heat generation or absorption. At low value of q, volumetric heat absorption is more dominant than heat generation. The bottom wall of cavity is cold at low value of q. Flow of heat increases as the value of q is increased, i.e., more prominant at higher value of q, i.e., $q = 10$.

The average Nusselt number distribution is demonstrated in Figure 3.8(a), with Hartmann number at various Richardson number. The values of Hartmann number are inversely proportional to mean Nusselt number. Noticeable convection is observed at higher values of Richardson number. Figure 3.8(b) illustrates that increase in nanoparticle volume fraction enhanced the Nu_{avg} and it remains linear for high value of Richardson number. Figure 3.8(c) depicts that the Nu_{avg} is enhanced linearly with volume fraction ϕ. Maximum heat transfer occured at low value of heat absorption parameter. Figure 3.8(d) portrays the impact of inclined magnetic field with variation in Hartmann number on mean Nusselt number. The heat transfer is reduced with an augmentation in inclined magnetic field and Hartmann number.

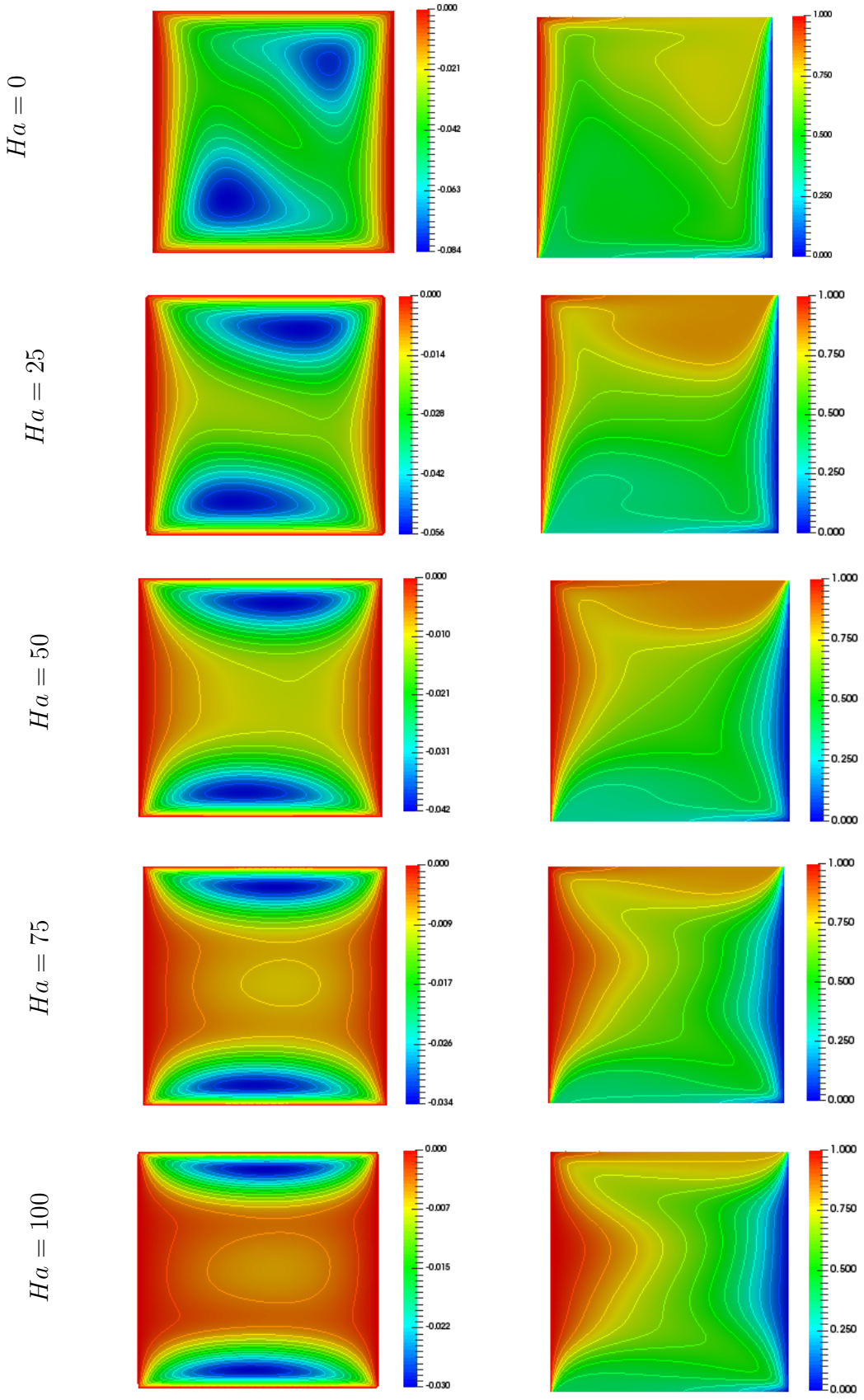

FIGURE 3.3: Influence of Ha on isotherms (right) and streamlines (left) with $q = 5$, $\gamma = 0°$, $\phi = 0.04$, $Re = 100$, $Ri = 5$.

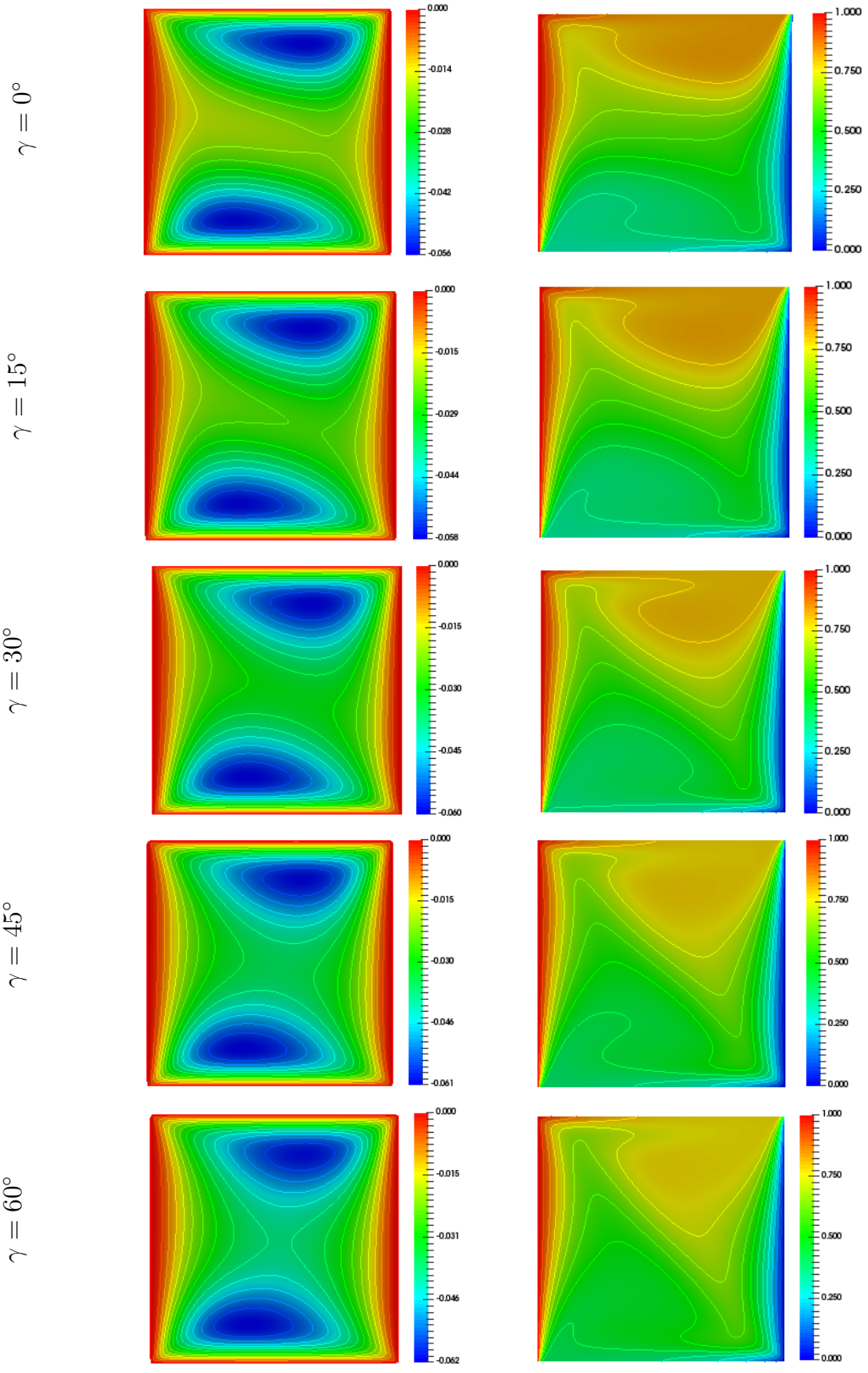

FIGURE 3.4: Influence of inclined magnetic field on streamlines (left) and isotherms (right) with $q = 5$, $\phi = 0.04$, $Ri = 5$, $Re = 100$, $Ha = 25$.

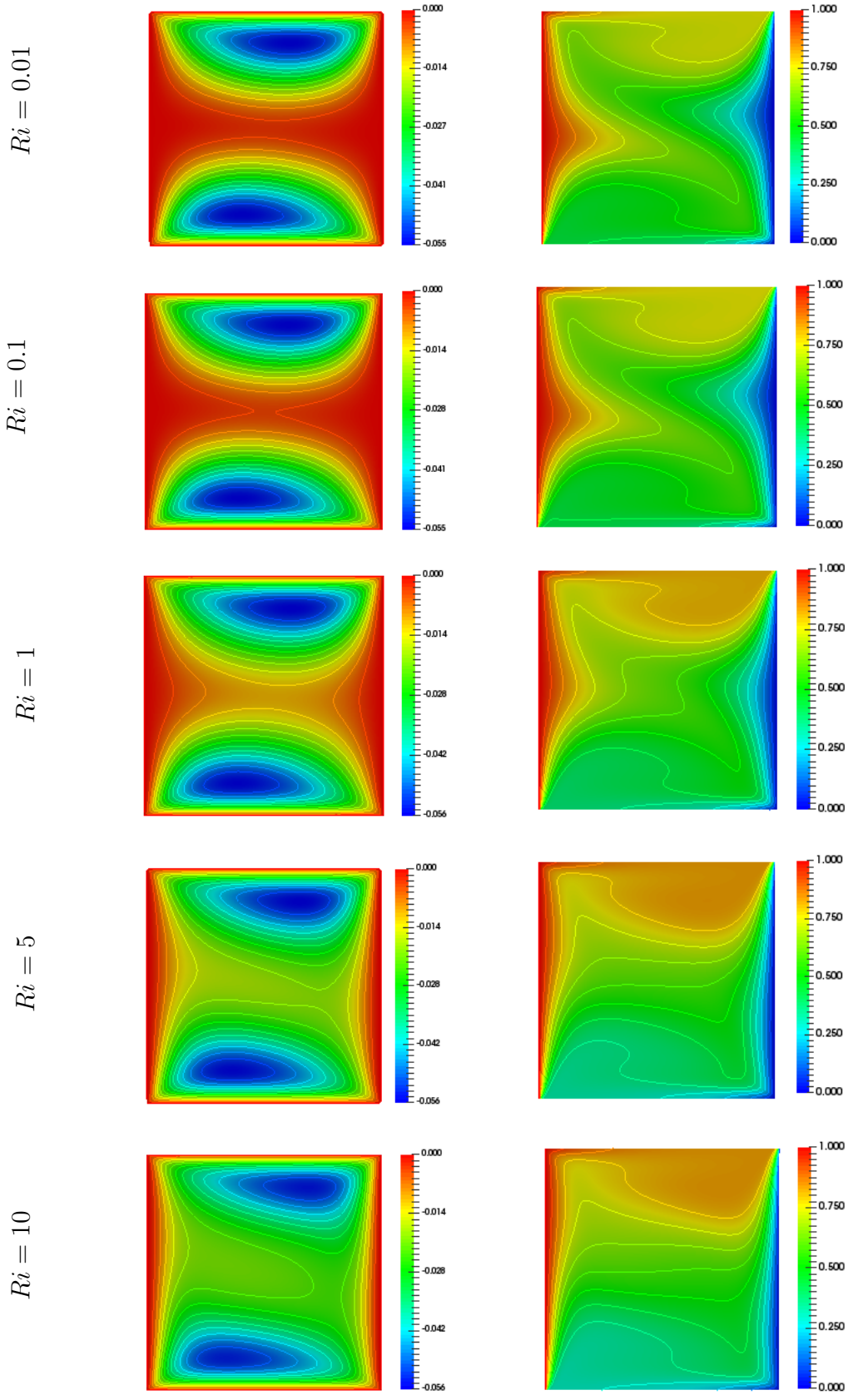

FIGURE 3.5: Influence of Ri on streamlines (left) and isotherms (right) with $\phi = 0.04$, $\gamma = 0°$, $Re = 100$, $q = 5$, $Ha = 25$.

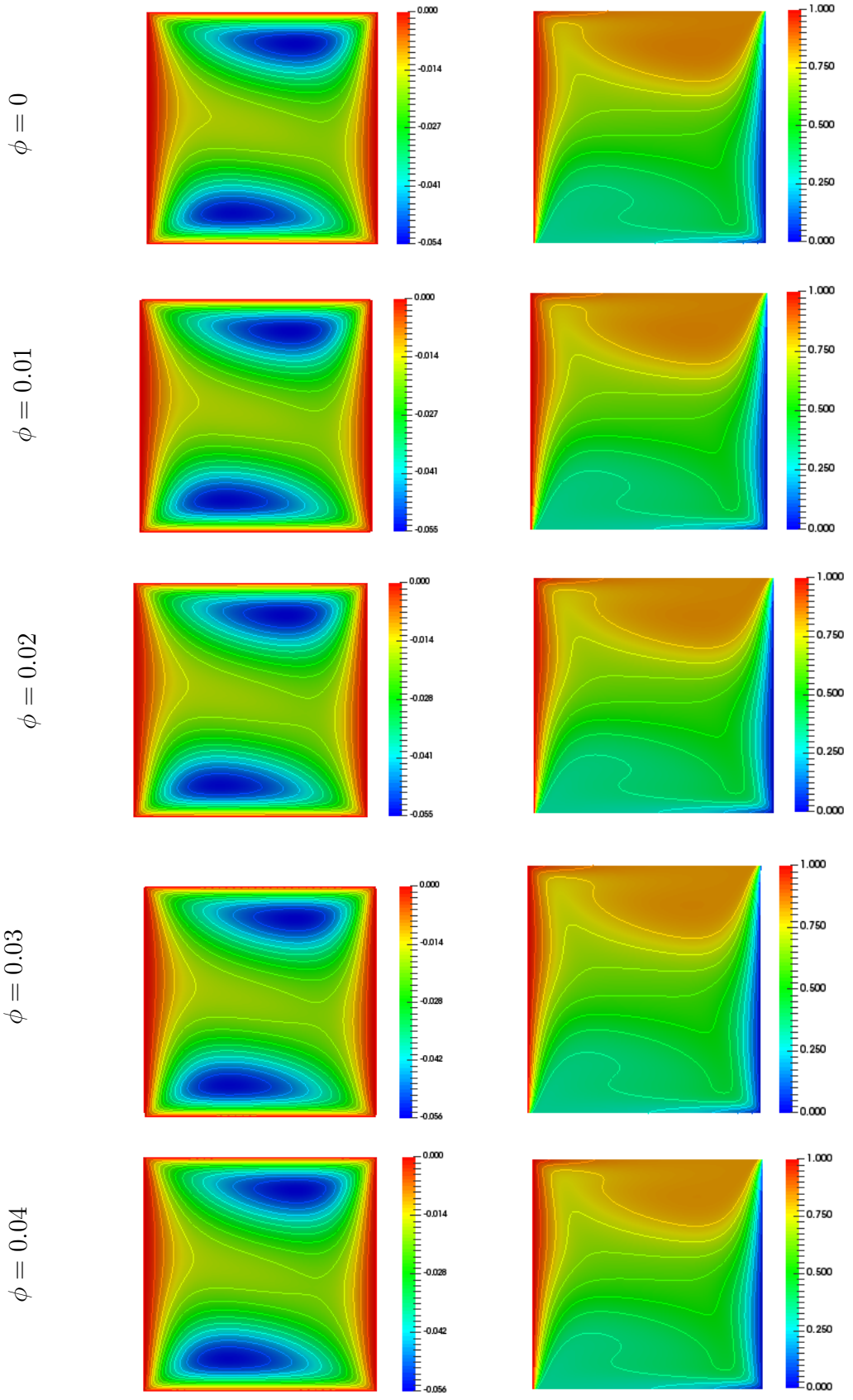

FIGURE 3.6: Influence of nanoparticles volume fraction on isotherms (right) and streamlines (left) with $Ri = 5$, $\gamma = 0°$, $Ha = 25$, $q = 5$, $Re = 100$.

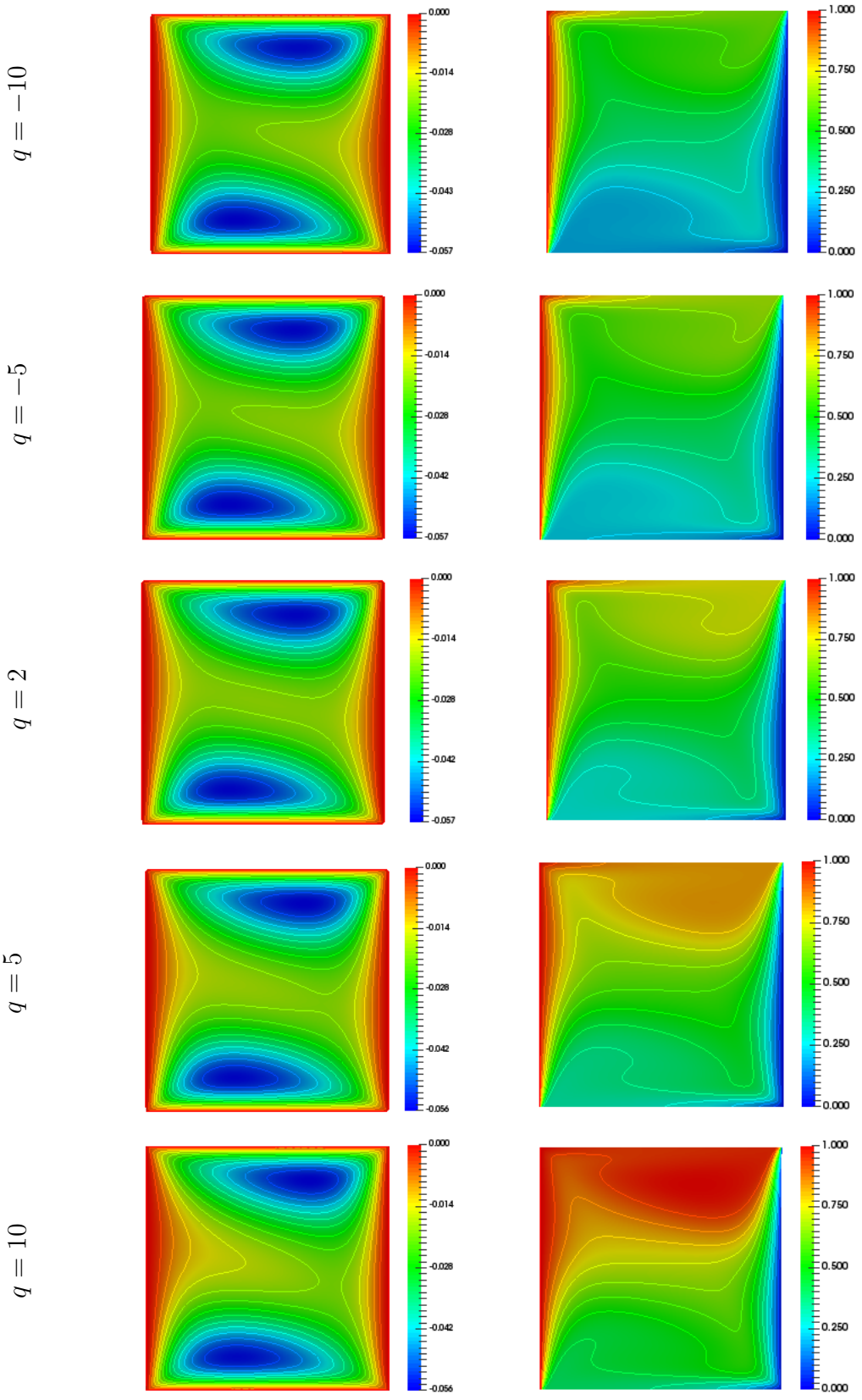

FIGURE 3.7: Influence of volumetric heat parameters on streamlines (left) and isotherms (right) with $\phi = 0.04$, $\gamma = 0°$, $Ri = 5$, $Re = 100$, $Ha = 25$.

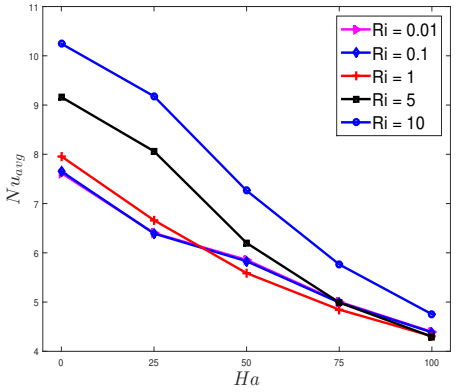

(a)

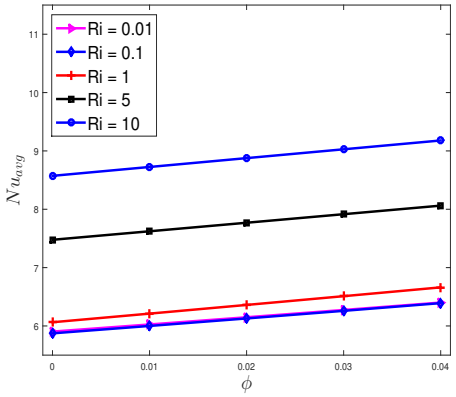

(b)

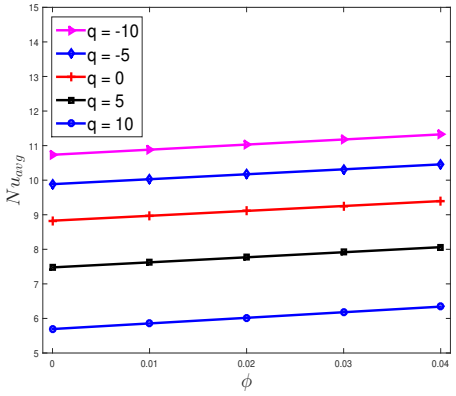

(c)

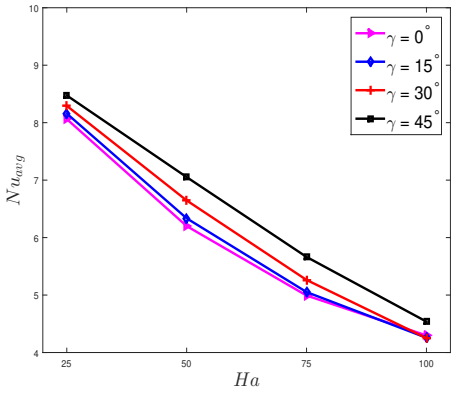

(d)

FIGURE 3.8: Effect of Ri on Nu_{avg} as a function of Hartmann number and nanoparticle volume fraction (a-b), impact of q on Nu_{avg} (c) and influence of γ on Nu_{avg} (d).

Chapter 4

Impact of Inclined Magnetic Field on Mixed Convective Nanofluid Flow with Porous Medium

In this chapter the extension is accomplished to the previous work of Hussain et al. [2]. Porous medium has significant role in convection process. For this purpose, we will analyze the influence of magnetic field inclination with the addition of homogeneous porous medium inside square cavity on the thermal energy transportation process. The results are portrayed in the form of streamlines, isotherms and useful plots at the end.

4.1 The Problem Configuration

The flow problem is analyzed inside a square shaped cavity. The problem configuration is presented in Figure 4.1. The fluid throughout the study is two dimensional, Newtonian, incompressible and viscous. Changes in flow behaviour w.r.t time are ignored, i.e., flow is assumed to be steady. Geometrical interpretation shows that the vertical left side of cavity is at high temperature i.e., T_h while the right side is kept cold i.e., T_c. The upper lid of cavity is moving with

velocity $u_0\ ms^{-1}$ while the horizontal lower side is moving with constant velocity of $-u_0\ ms^{-1}$. Both horizontal upper and lower sides are thermally insulated. Homogeneous porous medium is implanted in cavity region. Magnetic field of strength B_0 is inclining with angle γ°. Density variations are significant here due to temperature differences. To overcome this, Boussinesq approximation is used.

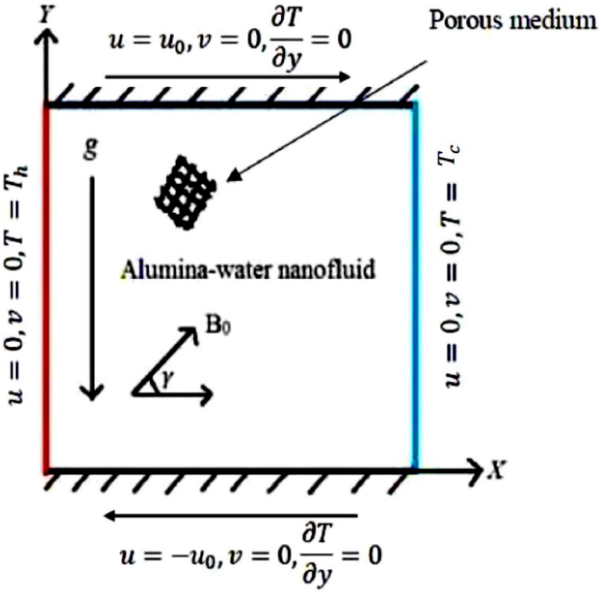

FIGURE 4.1: Configuration of physical model.

4.2 Governing Equations

From the above assumptions, the dimensional formulation of this governing phenomenon is written below. This set of four PDEs consist of continuity, momentum and energy equations [15, 16, 33]:

- Continuiy Equation:

$$\frac{\partial u}{\partial x} + \frac{\partial v}{\partial y} = 0, \tag{4.1}$$

- u-Momentum Equation:

$$\begin{aligned}\frac{1}{\epsilon^2}\left(u\frac{\partial u}{\partial x}+v\frac{\partial u}{\partial y}\right)=&-\frac{1}{\rho_{nf}}\frac{\partial p}{\partial x}+\frac{\mu_{nf}}{\rho_{nf}\epsilon}\left(\frac{\partial^2 u}{\partial x^2}+\frac{\partial^2 u}{\partial y^2}\right)\\&+\frac{B_0^2\sigma_{nf}}{\rho_{nf}}(v\sin\gamma\cos\gamma-u\sin\gamma^2)\\&-\frac{\mu_{nf}}{\rho_{nf}K}u-\frac{1.75}{\sqrt{150K}\epsilon^{\frac{3}{2}}}\left(\sqrt{u^2+v^2}\right)u,\end{aligned}\tag{4.2}$$

- v-Momentum Equation:

$$\begin{aligned}\frac{1}{\epsilon^2}\left(u\frac{\partial v}{\partial x}+v\frac{\partial v}{\partial y}\right)=&-\frac{1}{\rho_{nf}}\frac{\partial p}{\partial y}+\frac{\mu_{nf}}{\rho_{nf}\epsilon}\left(\frac{\partial^2 v}{\partial x^2}+\frac{\partial^2 v}{\partial y^2}\right)+\frac{(\rho\beta)_{nf}}{\rho_{nf}}g(T-T_c)\\&+\frac{B_0^2\sigma_{nf}}{\rho_{nf}}(u\sin\gamma\cos\gamma-v\cos^2\gamma)\\&-\frac{\mu_{nf}}{\rho_{nf}K}v-\frac{1.75}{\sqrt{150K}\epsilon^{\frac{3}{2}}}\left(\sqrt{u^2+v^2}\right)v,\end{aligned}\tag{4.3}$$

- Energy Equation:

$$u\frac{\partial T}{\partial x}+v\frac{\partial T}{\partial y}=\alpha_{nf}\left(\frac{\partial^2 T}{\partial x^2}+\frac{\partial^2 T}{\partial y^2}\right)+\frac{Q_0}{(\rho C_p)_{nf}}(T-T_c).\tag{4.4}$$

The corresponding boundary conditions related to the above PDEs (4.1) to (4.4) are mentioned below

- Upper horizontal side:

$$u=u_0,\qquad v=0,\qquad \frac{\partial T}{\partial y}=0.$$

- Lower horizontal side:

$$u=-u_0,\qquad v=0,\qquad \frac{\partial T}{\partial y}=0.$$

- Vertical left side:

$$u=0,\qquad v=0,\qquad T=T_h.$$

- Vertical right side:

$$u = 0, \qquad v = 0, \qquad T = T_c.$$

Effective properties of the nanofluid are discussed in equations (3.5), (3.6), (3.12).

4.3 Dimensionless Governing Equations

The governing system can be changed into dimensionless system by using the given dimensionless parameters [2, 16]:

$$\theta = \frac{T - T_c}{T_h - T_c}, \quad U = \frac{u}{u_0}, \quad Y = \frac{y}{L}, \quad V = \frac{v}{u_0}, \quad X = \frac{x}{L}, \quad P = \frac{p}{\rho_{nf} u_0^2},$$
$$Da = \frac{k}{L^2}, \quad Re = \frac{u_0 L}{\nu_f}, \quad Gr = \frac{g\beta_f \triangle T L^3}{\nu_f^2}, \quad Pr = \frac{\nu_f}{\alpha_f}, \quad q = \frac{Q_0 L^2}{(\rho C_p)_{nf}\alpha_f}$$
$$Ha = B_0 L\sqrt{\frac{\sigma_f}{\mu_f}}.$$

By using the above mentioned dimensionless physical parameters, the dimensional PDEs from (4.1) to (4.4) is transformed into the following dimensionless system.

$$\frac{\partial U}{\partial X} + \frac{\partial V}{\partial Y} = 0, \tag{4.5}$$

$$\begin{aligned}\frac{1}{\epsilon^2}\left(U\frac{\partial U}{\partial X} + V\frac{\partial U}{\partial Y}\right) = &-\frac{\partial P}{\partial X} + \frac{1}{Re}\frac{\rho_f}{\rho_{nf}}\frac{1}{\epsilon(1-\phi)^{2.5}}\left(\frac{\partial^2 U}{\partial X^2} + \frac{\partial^2 U}{\partial Y^2}\right)\\ &- \frac{\mu_{nf}}{\rho_{nf}\nu_f}\frac{1}{ReDa}U - \frac{1.75}{\sqrt{150Da\epsilon^3}}\left(\sqrt{U^2+V^2}\right)U\\ &+ \frac{\rho_f}{\rho_{nf}}\frac{\sigma_{nf}}{\sigma_f}\frac{Ha^2}{Re}(V\sin\gamma\cos\gamma - U\sin^2\gamma),\end{aligned} \tag{4.6}$$

$$\begin{aligned}\frac{1}{\epsilon^2}\left(U\frac{\partial V}{\partial X} + V\frac{\partial V}{\partial Y}\right) = &-\frac{\partial P}{\partial Y} + \frac{1}{Re}\frac{\rho_f}{\rho_{nf}}\frac{1}{\epsilon(1-\phi)^{2.5}}\left(\frac{\partial^2 V}{\partial X^2} + \frac{\partial^2 V}{\partial Y^2}\right)\\ &- \frac{\mu_{nf}}{\rho_{nf}\nu_f}\frac{1}{ReDa}V - \frac{1.75}{\sqrt{150Da\epsilon^3}}\left(\sqrt{U^2+V^2}\right)V\\ &+ Ri\frac{\rho_f}{\rho_{nf}}\left(1 - \phi + \frac{\rho_s\beta_s}{\rho_f\beta_f}\phi\right)\theta\\ &+ \frac{\sigma_{nf}}{\sigma_f}\frac{\rho_f}{\rho_{nf}}\frac{Ha^2}{Re}(U\sin\gamma\cos\gamma - V\cos^2\gamma),\end{aligned} \tag{4.7}$$

$$U\frac{\partial\theta}{\partial X}+V\frac{\partial\theta}{\partial Y}=\frac{\alpha_{nf}}{\alpha_f}\frac{1}{RePr}\left(\frac{\partial^2\theta}{\partial X^2}+\frac{\partial^2\theta}{\partial Y^2}\right)+\frac{1}{RePr}q\theta. \tag{4.8}$$

Following conditions on boundaries are related to the above system of Eqs. (4.5) to Eq. (4.8).

- Upper horizontal side:

$$V=0, \qquad U=1, \qquad \frac{\partial\theta}{\partial y}=0.$$

- Lower horizontal side:

$$V=0 \qquad U=-1, \qquad \frac{\partial\theta}{\partial y}=0.$$

- Vertical left side:

$$V=0, \qquad U=0, \qquad \theta=1.$$

- Vertical right side:

$$V=0, \qquad U=0, \qquad \theta=0.$$

4.4 Numerical Solution

The numerical solution of non-dimensional equations is obtained by using finite element method. Galerkin's residual method is applied here to achieve the weak formulation of the coupled equations from (4.5) to (4.8) with the respective boundary conditions. The non-linear equations are discretized into quadtrilateral elements in whole domain (Ω). For this purpose, first of all find the weak form of the equations. Following are the main steps of solution procedure:

4.4.1 Variation Formulation

The basic attribute of finite element method is to convert the strong form of governing equations into weak form. For variational formulation, governing equations

are multiplied by test functions and integrate over the whole domain Ω.

The strong form of governing system of equations from (4.5) to (4.8) is given below

$$\frac{\partial U}{\partial X}+\frac{\partial V}{\partial Y}=0, \tag{4.9}$$

$$A_1\left(U\frac{\partial U}{\partial X}+V\frac{\partial U}{\partial Y}\right)=-\frac{\partial P}{\partial X}+A_2\left(\frac{\partial^2 U}{\partial X^2}+\frac{\partial^2 U}{\partial Y^2}\right)-A_4U + A_3(V\sin\gamma\cos\gamma-U\sin^2\gamma)-A_5U, \tag{4.10}$$

$$A_1\left(U\frac{\partial V}{\partial X}+V\frac{\partial V}{\partial Y}\right)=-\frac{\partial P}{\partial Y}+A_2\left(\frac{\partial^2 V}{\partial X^2}+\frac{\partial^2 V}{\partial Y^2}\right)-A_4V + A_3\left(U\sin\gamma\cos\gamma-V\cos^2\gamma\right)-A_5V+A_6\theta, \tag{4.11}$$

$$U\frac{\partial \theta}{\partial X}+V\frac{\partial \theta}{\partial Y}=A_7\left(\frac{\partial^2 \theta}{\partial X^2}+\frac{\partial^2 \theta}{\partial Y^2}\right)+A_8\theta. \tag{4.12}$$

In the above equations, A_i's are given below

$$A_1=\frac{1}{\epsilon^2},\quad A_2=\frac{1}{Re}\frac{\rho_f}{\rho_{nf}}\frac{1}{\epsilon(1-\phi)^{2.5}},\quad A_6=Ri\frac{\rho_f}{\rho_{nf}}\left(1-\phi+\frac{\rho_s\beta_s}{\rho_f\beta_f}\phi\right),$$
$$A_4=\frac{\mu_{nf}}{\rho_{nf}\nu_f}\frac{1}{ReDa},\quad A_5=\frac{1.75}{\sqrt{150Da}\epsilon^{\frac{3}{2}}}\left(\sqrt{U^2+V^2}\right),\quad A_3=\frac{\rho_f}{\rho_{nf}}\frac{\sigma_{nf}}{\sigma_f}\frac{Ha^2}{Re},$$
$$A_7=\frac{\alpha_{nf}}{\alpha_f}\frac{1}{RePr},\quad A_8=\frac{1}{RePr}.$$

Let $\mathbf{W}=[H_1(\Omega)]^3$ be the test spaces for velocity components (U,V) and temperature θ, $Q=L_2(\Omega)$ refers to the test space for pressure P component. Let $w\,\epsilon\,\mathbf{W}$ and $q\,\epsilon\,Q$ are the respective test functions for the test spaces. For variation formulation multiply momentum and energy equation with test function w. Similarly multiply q test function with continuity equation.

Find $(U, V, \theta, P)\,\epsilon\,\mathbf{W}\times Q$ such that

$$A_1\left(U\frac{\partial U}{\partial X}+V\frac{\partial U}{\partial Y}\right)wd\Omega+\int_\Omega\frac{\partial P}{\partial X}wd\Omega-A_2\int_\Omega\left(\frac{\partial^2 U}{\partial X^2}+\frac{\partial^2 U}{\partial Y^2}\right)wd\Omega$$
$$-A_3\int_\Omega(V\sin\gamma\cos\gamma-U\sin^2\gamma)wd\Omega+A_4\int_\Omega Uwd\Omega+A_5\int_\Omega Uwd\Omega=0, \quad (4.13)$$

$$A_1\int_\Omega\left(U\frac{\partial V}{\partial X}+V\frac{\partial V}{\partial Y}\right)wd\Omega+\int_\Omega\frac{\partial P}{\partial Y}wd\Omega-A_2\int_\Omega\left(\frac{\partial^2 V}{\partial X^2}+\frac{\partial^2 V}{\partial Y^2}\right)wd\Omega$$
$$-A_6\int_\Omega\theta wd\Omega-A_3\int_\Omega(U\sin\gamma\cos\gamma-V\cos^2\gamma)wd\Omega+A_4\int_\Omega Vwd\Omega$$
$$+A_5\int_\Omega Vwd\Omega=0, \quad (4.14)$$

$$\int_\Omega\frac{\partial U}{\partial X}qd\Omega+\int_\Omega\frac{\partial V}{\partial Y}qd\Omega=0, \quad (4.15)$$

$$\int_\Omega\left(U\frac{\partial\theta}{\partial X}+V\frac{\partial\theta}{\partial Y}\right)wd\Omega-A_7\int_\Omega\left(\frac{\partial^2\theta}{\partial X^2}+\frac{\partial^2\theta}{\partial Y^2}\right)wd\Omega-A_8\int_\Omega\theta wd\Omega=0. \quad (4.16)$$

$\forall\,(w,q)\;\epsilon\,\mathbf{W}\times Q$

Let $\theta\approx\theta_h,\ V\approx V_h,\ q\approx q_h,\ U\approx U_h,\ w\approx w_h,\ P\approx P_h$

By Galerkin's approximation method

$$A_2\int_\Omega\left(\frac{\partial U_h}{\partial X}\frac{\partial w_h}{\partial X}+\frac{\partial U_h}{\partial Y}\frac{\partial w_h}{\partial Y}\right)d\Omega+A_1\int_\Omega\left(U_h\frac{\partial U_h}{\partial X}+V_h\frac{\partial U_h}{\partial Y}\right)w_hd\Omega$$
$$+A_4\int_\Omega U_hw_hd\Omega+A_5\int_\Omega U_hw_hd\Omega-\int_\Omega\frac{\partial w_h}{\partial X}P_hd\Omega+\omega_1\int_\Omega U_hw_hd\Omega$$
$$-\omega_2\int_\Omega V_hw_hd\Omega=0, \quad (4.17)$$

$$A_2\int_\Omega\left(\frac{\partial V_h}{\partial X}\frac{\partial w_h}{\partial X}+\frac{\partial V_h}{\partial Y}\frac{\partial w_h}{\partial Y}\right)d\Omega+A_1\int_\Omega\left(U_h\frac{\partial V_h}{\partial X}+V_h\frac{\partial V_h}{\partial Y}\right)w_hd\Omega$$
$$+A_4\int_\Omega V_hw_hd\Omega+A_5\int_\Omega V_hw_hd\Omega-\int_\Omega\frac{\partial w_h}{\partial Y}P_hd\Omega-\omega_2\int_\Omega U_hw_hd\Omega$$
$$+\omega_3\int_\Omega V_hw_hd\Omega-A_6\int_\Omega\theta_hw_hd\Omega=0, \quad (4.18)$$

$$\int_\Omega\frac{\partial U_h}{\partial X}q_hd\Omega+\int_\Omega\frac{\partial V_h}{\partial Y}q_hd\Omega=0, \quad (4.19)$$

$$\int_\Omega \left(U_h \frac{\partial \theta_h}{\partial X} + V_h \frac{\partial \theta_h}{\partial Y}\right) w_h d\Omega + A_7 \int_\Omega \left(\frac{\partial \theta_h}{\partial X}\frac{\partial w_h}{\partial X} + \frac{\partial \theta_h}{\partial Y}\frac{\partial w_h}{\partial Y}\right) d\Omega$$
$$- A_8 \int_\Omega \theta_h w_h d\Omega = 0, \tag{4.20}$$

where ω_i's in above equations are represented as

$$\omega_1 = A_3 \sin^2\gamma, \qquad \omega_2 = A_3 \sin\gamma\cos\gamma, \qquad \omega_3 = A_3 \cos^2\gamma.$$

The equations from (4.17) to (4.20) are approximated by using the FEM approximation functions for trial spaces and test spaces are given below

$$U_h = \sum_{j=1}^{n} U_j S_j, \quad V_h = \sum_{j=1}^{n} V_j S_j, \quad P_h = \sum_{j=1}^{m} P_j \eta_j, \quad \theta_h = \sum_{j=1}^{n} \theta_j S_j$$
$$w_h = \sum_{i=1}^{n} w_i S_i, \quad q_h = \sum_{i=1}^{m} q_i \eta_i.$$

Now inserting the approximate functions of test and trial spaces in equations (4.17) to (4.20), the matrix form of discretized system is

$$\begin{pmatrix} K^{11} & K^{12} & K^{13} & K^{14} \\ K^{21} & K^{22} & K^{23} & K^{24} \\ K^{31} & K^{32} & K^{33} & K^{34} \\ K^{41} & K^{42} & K^{43} & K^{44} \end{pmatrix} \begin{pmatrix} \underline{U} \\ \underline{V} \\ \underline{P} \\ \underline{\theta} \end{pmatrix} = \begin{pmatrix} \underline{F^1} \\ \underline{F^2} \\ \underline{F^3} \\ \underline{F^4} \end{pmatrix}, \tag{4.21}$$

where$\underline{\theta} = \theta_j, \underline{V} = V_j, \underline{U} = U_j;\ j = 1, 2, \ldots, n$, and $\underline{P} = P_j;\ j = 1, 2, \ldots, m$. The vectors $\underline{F^1}, \ldots, \underline{F^4}$ represent the corresponding R.H.S. The corresponding block matrices are

$$K^{11}{}_{ij} = A_1 \int_\Omega \left(\sum_{j=1}^{n} U_j S_j \frac{\partial S_j}{\partial X} + \sum_{j=1}^{n} V_j S_j \frac{\partial S_j}{\partial Y}\right) S_i d\Omega + A_2 \int_\Omega \left(\frac{\partial S_j}{\partial X}\frac{\partial S_i}{\partial X} + \frac{\partial S_j}{\partial Y}\frac{\partial S_i}{\partial Y}\right) d\Omega$$
$$+ A_4 \int_\Omega S_j S_i d\Omega + A_5 \int_\Omega S_j S_i d\Omega + \omega_1 \int_\Omega S_j S_i d\Omega,$$

$$K^{22}{}_{ij} = A_1 \int_\Omega \left(\sum_{j=1}^{n} U_j S_j \frac{\partial S_j}{\partial X} + \sum_{j=1}^{n} V_j S_j \frac{\partial S_j}{\partial Y}\right) S_i d\Omega + A_2 \int_\Omega \left(\frac{\partial S_j}{\partial X}\frac{\partial S_i}{\partial X} + \frac{\partial S_j}{\partial Y}\frac{\partial S_i}{\partial Y}\right) d\Omega$$
$$+ A_4 \int_\Omega S_j S_i d\Omega + A_5 \int_\Omega S_j S_i d\Omega + \omega_3 \int_\Omega S_j S_i d\Omega,$$

$$K^{44}{}_{ij} = \int_\Omega \left(\sum_{j=1}^{n} U_j S_j \frac{\partial S_j}{\partial X} + \sum_{j=1}^{n} V_j S_j \frac{\partial S_j}{\partial Y} \right) S_i d\Omega + A_7 \int_\Omega \left(\frac{\partial S_j}{\partial X}\frac{\partial S_i}{\partial X} + \frac{\partial S_j}{\partial Y}\frac{\partial S_i}{\partial Y} \right) d\Omega$$
$$- A_8 \int_\Omega S_j S_i d\Omega,$$

$$K^{12}{}_{ij} = -\omega_2 \int_\Omega S_j S_i d\Omega = K^{21}{}_{ij}, \quad K^{13}{}_{ij} = -\int_\Omega \frac{\partial S_i}{\partial X}\eta_j d\Omega, \quad K^{23}{}_{ij} = -\int_\Omega \frac{\partial S_i}{\partial Y}\eta_j d\Omega$$

$$K^{24}{}_{ij} = -A_6 \int_\Omega S_j S_i d\Omega, \quad K^{31}{}_{ij} = \int_\Omega \frac{\partial S_j}{\partial X}\eta_i d\Omega, \quad K^{32}{}_{ij} = \int_\Omega \frac{\partial S_j}{\partial Y}\eta_i d\Omega$$

$$K^{14}{}_{ij} = K^{33}{}_{ij} = K^{34}{}_{ij} = K^{41}{}_{ij} = K^{42}{}_{ij} = K^{43}{}_{ij} = 0.$$

The system of non-linear equations is linearized by using Picard method while the linearized algebraic equations are solved by using Gaussian elimination scheme to achieve approximated solution. In order to obtain the convergence of approximated solution, the stopping criterion will remain same for the present case as discussed in **Chaper** 3.

4.5 Results and Discussion

The influence of inclined magnetic field on mixed convection of nanofluid filled in double lid driven enclosure with porous medium has been studied numerically for different parameters.

The influence of variation in Hartmann number on heat transfer process with $\gamma = 0°$, $\phi = 0.04$, $Ri = 5$, $Re = 100$, $q = 5$ and $Da = 10^{-3}$ is depicts in Figure 4.2. In the absence of magnetic field at $Ha = 0$, streamlines are less concentrated with top lid and bottom lid of cavity with a visible flow activity due to greater kinetic energy (K.E) of fluid in the center of cavity. As the strength of magnetic field increases, these concentric cells grows with the top and bottom lids, showing the reduced flow circulation in the center of cavity. This effect is more prominant at the highest value of Hartmann number, i.e., $Ha = 100$. For this value of Ha strength of Lorentz force is dominated on this buoyancy-driven flow. The flow activity seems to retard at the central region due to less kinetic energy (K.E) of

fluid at this high strength of magnetic force. Thin thermal layer is noticed with the left wall in isotherms of Figure 4.2 at $Ha = 0$ and 25. Heat layer seems more visible and consequently shifting towards the top lid. Cold region at the bottom increases in this regard. At the highest value of magnetic field i.e., $Ha = 100$, more visible heat layers are distinctly seen with the left wall of cavity. Here the heat movement is confined from left wall to the top lid of cavity without affecting the bottom side and right wall. Hence less convection is observed at this high strength of Lorentz force. Increment in Hartmann number facilitates prominant volumetric heat generation.

Effect of Richardson number with $Ri = 0.01, 0.1, 1, 5$, and 10 are shown in Figure 4.3. The forced convection is dominated at the low values of Ri on flow characteristics. Due to greater strength of shear forces more cells are formed with the top lid and at the bottom lid. Lids movement is aiding this strength. Influence of buoyancy force dominates for increasing Richardson number. At this stage, the rotating cells start to vanish which produces a weak flow activity at the central portion of cavity. Here most of the streamlines start accumulate at the left and right sides. Isotherms in Figure 4.3 distinctly depicts the heat flow inside square cavity. At forced convection dominated flow, thick thermal layer is developed with left wall and this effect reduces gradually as Ri increases. For natural convective flow, thin thermal layers are found with left wall showing the presence of less heat energy due to high buoyancy force effects. A visible volumetric heat absorption is analyzed for the increased value of Ri.

Influence of Darcy number with $\phi = 0.04$, $\gamma = 0°$, $Re = 100$, $q = 5$, $Ri = 5$ and $Ha = 25$ is presented in Figure 4.4. For low Darcy numbers, i.e., $Da = 10^{-5}$ and 10^{-4}, drag forces enhanced due to least permeability for which more merged rotating cells are formed at the moving horizontal upper and lower lids. Hence weak flow circulation is seemed at the center cavity due to the domination of resistive forces of medium. At $Da = 10^{-3}$, rotating cells are seemed with top and bottom lids with fine but weak flow movement from left to right wall of cavity. At the valued of $Da = 10^{-2}$ and 10^{-1}, increased flow movement is seen due to least effect of drag forces of porous medium. This impact is also influenced by

movement of horizontal upper and lower lids of cavity. Due to this an accelerated flow activity is distinctly viewed in central region. At these values permeability of medium increases with least effects of drag forces. Similar effects can be observed in the isotherms of Figure 4.4. For low value of Darcy number, thin merged heat layers are formed at the left wall and less absorption of heat is noticed due to high drag forces effects. Hence less heat transport activity is noticed. As Da grows up to 10^{-2} and 10^{-1}, noticeable thick heat layer is analyzed at the left wall which is constantly absorbed by moving top lid. Hence maximum temperature distribution is viewed at these values of Da.

Figure 4.5(a) portray the variations in Nu_{avg} with different Hartmann number for different modes of convection. It is noticed that Nu_{avg} decreases gradually with the increment in Ha. As in increasing Hartmann number the Lorentz force is enhanced and it reduces the speed of flow. Noticeable convection is observed at $Ri = 10$ due to the domination of buoyancy forces. Figure 4.5(b) shows differences in Nu_{avg} with the growing values of Darcy number. It is realized that Nu_{avg} increases at the rising values of Da. This variation become more significant for buoyancy-driven flow at $Ri = 5$ and 10. Figure 4.5(c) illustrates the variations in Nu_{avg} for different magnetic field inclination with varied Hartmann numbers. It is found that Nu_{avg} increases gradually with increasing magnetic field inclination. Most enhanced convection is viewed at $\gamma = 90^{\circ}$ for least magnetic field strength at $Ha = 25$. Hence with increasing Lorentz force strength Nu_{avg} decreases.

Figure 4.6(a) shows variations in θ_{avg} with increasing Hartmann number. Rise in θ_{avg} illustrate that the ratio of heat transfer through convection heat transfer by conduction decrease. This leads to the fact that conduction mode is dominating. Due to this average temperature distribution inside cavity increases espacially for $Ri = 5$ and 10. Moreover, natural convection is more significant for the rise in θ_{avg}. Figure 4.6(b) depicts the changes in θ_{avg} for increasing values of Da for all Ri. The heat transfer through convection dominates here for which average temperature decreases. Temperature distributes uniformly through out the cavity, due to the balance between resistive and buoyancy forces. Hence maximum θ_{avg} is recorded for mixed convection regime at $Ri = 1$. Figure 4.6(c) illustrates the θ_{avg} variations

with the magnetic field inclination at different Hartmann number. Enhanced convection is seen at $\gamma = 45^{\circ}$ for increased magnetic field strength, i.e., $Ha = 100$. This is due to the Lorentz forces which are retarding mode of convection. Hence heat transfer due to conduction becomes visible in the presence of Lorentz forces.

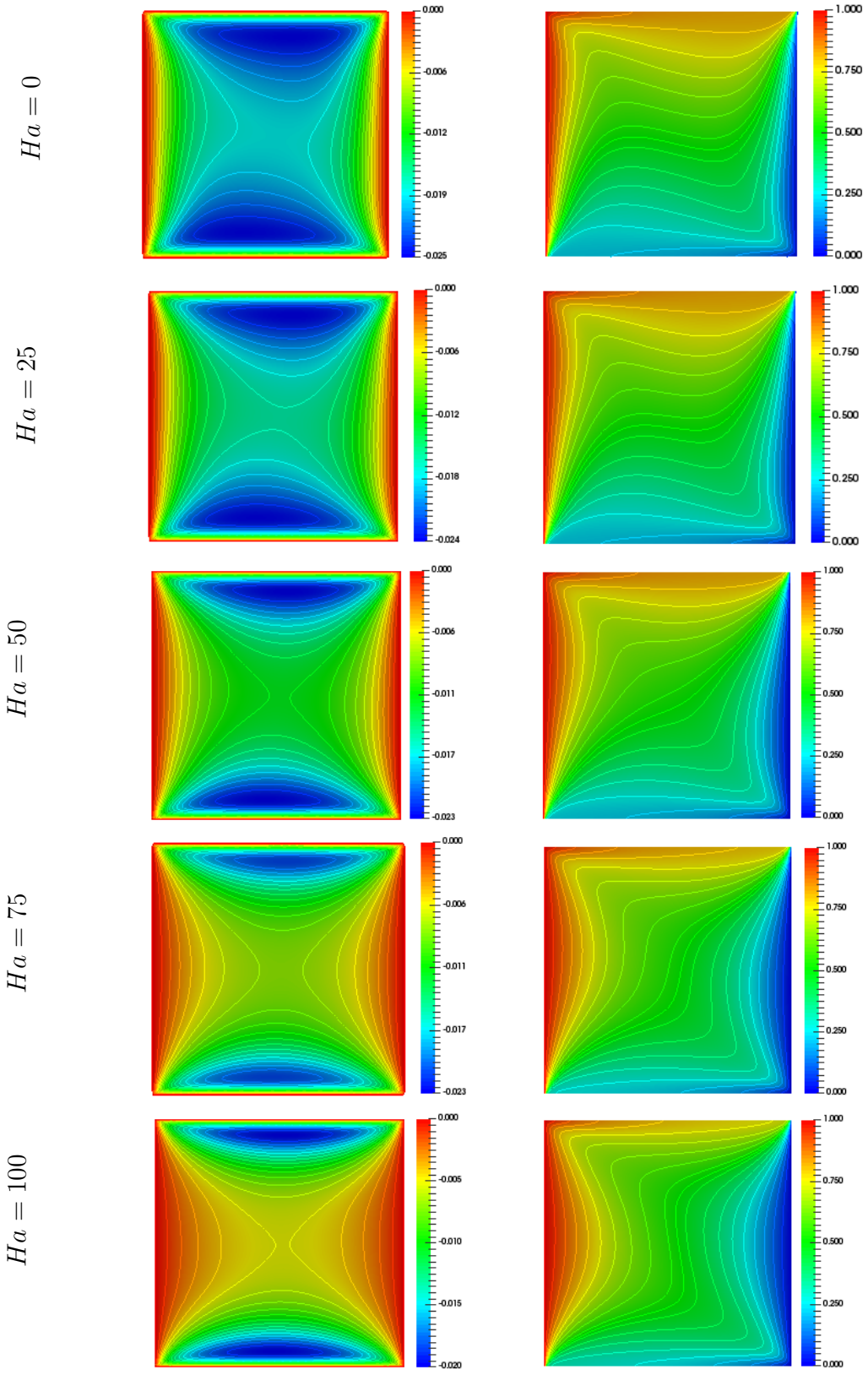

FIGURE 4.2: Influence of Hartmann number on streamlines (left) and isotherms (right) with $\gamma = 0°$, $Da = 10^{-3}$, $Ri = 5$, $Re = 100$, $q = 5$, $\phi = 0.04$.

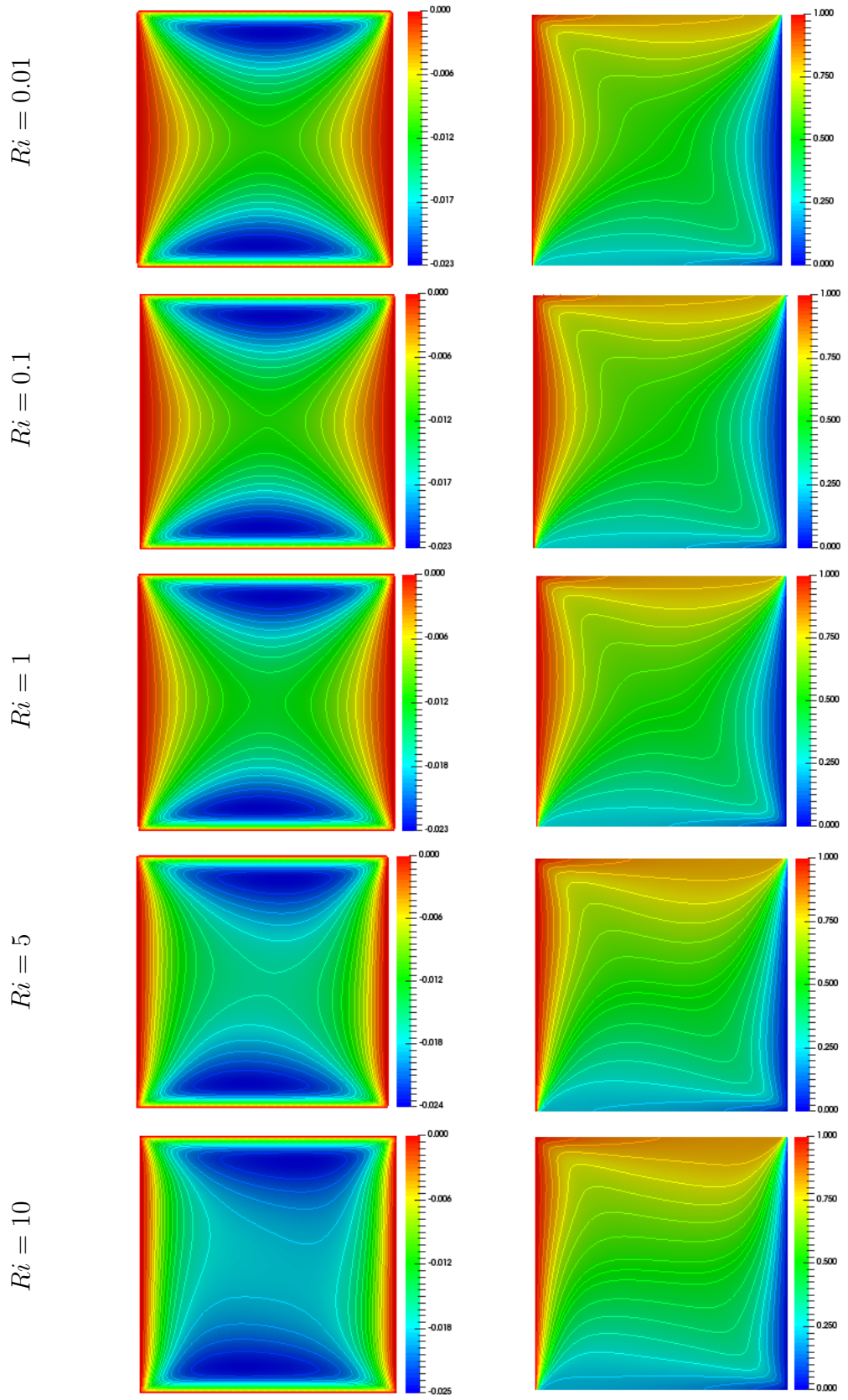

FIGURE 4.3: Influence of Richardson number on isotherms (right) and streamlines (left) with $\phi = 0.04$, $\gamma = 0°$, $Re = 100$, $q = 5$, $Ha = 25$, $Da = 10^{-3}$.

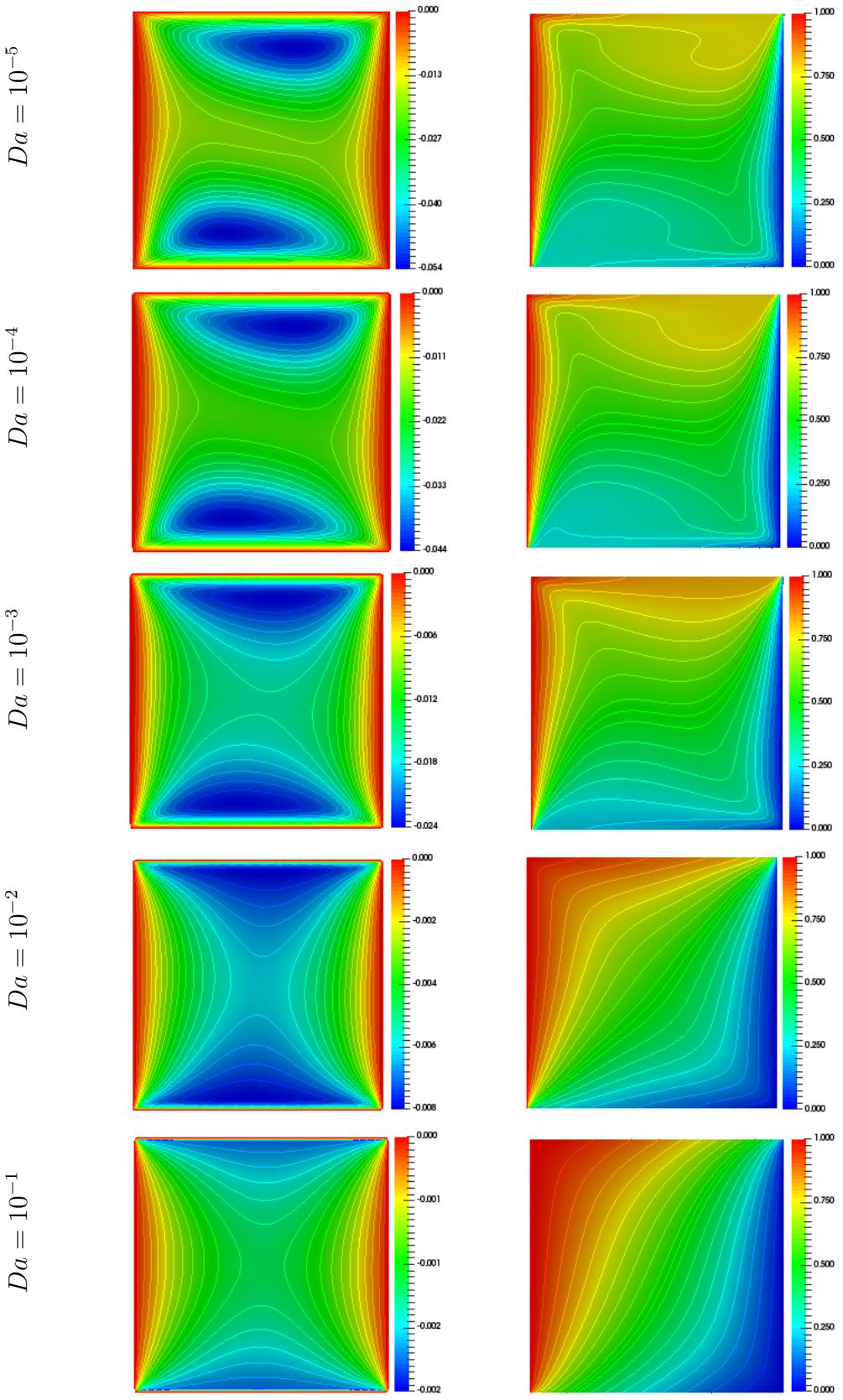

FIGURE 4.4: Influence of Darcy number on streamlines (left) and isotherms (right) with $\phi = 0.04$, $\gamma = 0°$, $q = 5$, $Ha = 25$, $Ri = 5$, $Re = 100$.

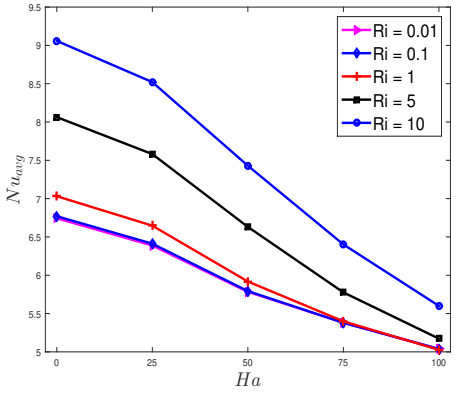

(a)

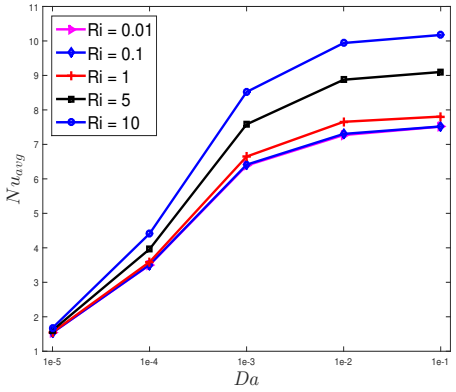

(b)

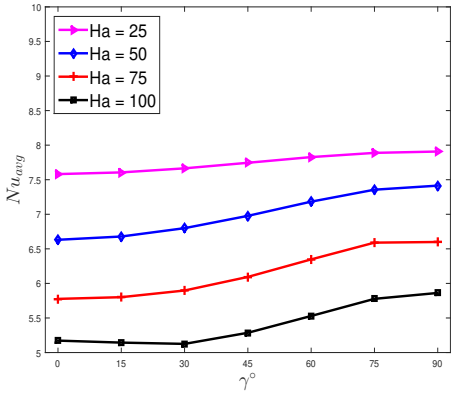

(c)

FIGURE 4.5: Influence of Ri on Nu_{avg} as a function of Hartmann number (a), impact of Darcy number on Nu_{avg} (b) and effect of inclined magnetic field on Nu_{avg} (c).

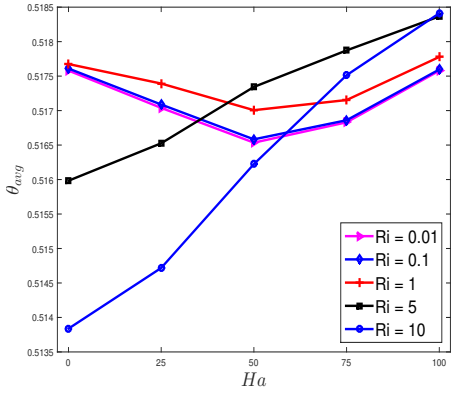

(a)

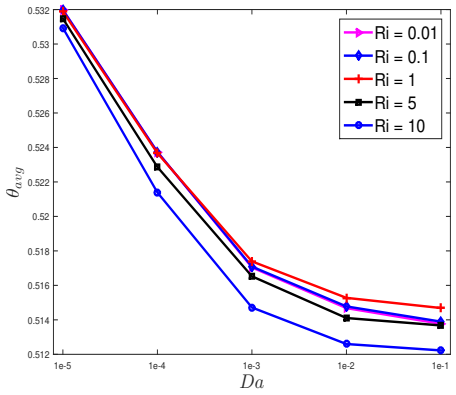

(b)

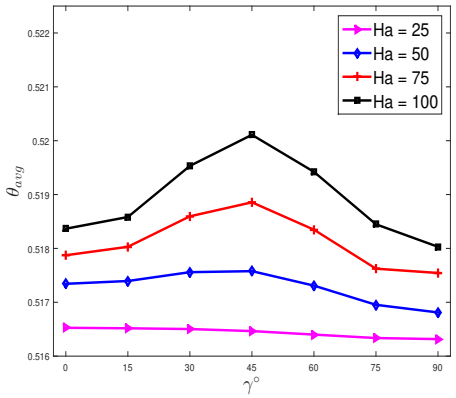

(c)

FIGURE 4.6: Impact of Ri on θ_{avg} as a function of Ha (a), effect of Da on θ_{avg} (b) and influence of inclined magnetic field on θ_{avg} (c).

Chapter 5

Conclusion

In this dissertation, the analysis of mixed convection of alumina-water nanofluid with porous medium under the influence of inclined magnetic field and internal heat parameters in a square cavity is investigated. Both the horizontal cavity walls are adiabatic whereas the left cavity wall exhibit hot temperature and right one has cold temperature. Furthermore square cavity has pourous medium. The dimensional equations are transformed into dimensionless form by using non-dimension variables and then discretized by using GFEM. We analyzed the impact of Hartmann, Richardson and Darcy numbers with the help of isotherms and streamlines. The graphical representation for average temperature and Nusselt number has also discussed.

In this study, a complete review of Hussain et al. [2] work is given. Also, the extension of this work is presented by using the concept of pourous medium. The average Nusselt number and temperature are examined to analyze convection process. Also, the heat distribution and flow behaviour have been investigated through streamlines and isotherms. From the present study, the following results are concluded;

- Less heat convection is observed at high strength of Lorentz force. Increase in Hartmann number facilitates prominant volumetric heat generation.

- Increase in Richardson number enhanced the thermal distribution flow where forced convection is dominated at low values of Richardson number. A visible volumetric heat absorption is analyzed for increased values of Richardson number.

- An augmentation in thermal distribution and flow movement is observed for high values of Darcy number due to the least effect of drag forces.

- Nu_{avg} decreases gradually with an increasing Hartmann number. Noticeable convection is observed at $Ri = 10$ due to the domination of buoyancy forces. Average temperature increases with rise in Hartmann number. It is more prominant for $Ri = 5$ and 10.

- Average Nusselt number grows for increasing values of Darcy number whereas this variation is more significant for buoyancy-driven flow as $Ri = 5$ and 10 while average temperature is decreases for augmentation in Darcy number for all Ri. Maximum average temperature is observed for mixed convection regime ar $Ri = 1$.

- A significant reduction in Nu_{avg} is observed with increasing Lorentz force strength. Most enhanced convection is viewed at $\gamma = 90°$ for least magnetic field strength at $Ha = 25$ whereas average temperature increases with the variation in magnetic field inclination at different Hartmann number. Enhanced convection is seen at $\gamma = 45°$ for increased magnetic field strength.

Bibliography

[1] D. Chatterjee. MHD mixed convection in a lid-driven cavity including a heated source. *An International Journal of Computation and Methodology*, 64:235–254, 2013.

[2] S. Hussain, H. F. Oztop, K. Mehmood, and N. Abu-Hamdeh. Effects of inclined magnetic field on mixed convection in a nanofluid filled double lid-driven cavity with volumetric heat generation or absorption using finite element method. *Chinese Journal of Physics*, 56(2):484 – 501, 2018. ISSN 0577-9073.

[3] GH. R. Kefayati. Effect of a magnetic field on natural convection in an open cavity subjected to water-alumina nanofluid using Lattice Boltzmann Method. *International Communications in Heat and Mass Transfer*, 40:67 – 77, 2013. ISSN 0735-1933.

[4] K. Al-Salem, H. F. Oztop, I. Pop, and Y. Varol. Effects of moving lid direction on MHD mixed convection in a linearly heated cavity. *International Journal of Heat and Mass Transfer*, 55(4):1103 – 1112, 2012. ISSN 0017-9310.

[5] S. Mondal and P. Sibanda. An unsteady double-diffusive natural convection in an inclined rectangular enclosure with different angles of magnetic field. *International Journal of Computational Methods*, 13(4):17, 2016.

[6] H. M. Elshehabey and S. E. Ahmed. MHD mixed convection in a lid-driven cavity filled by a nanofluid with sinusoidal temperature distribution on the both vertical walls using Buongiornos nanofluid model. *International Journal of Heat and Mass Transfer*, 88:181 – 202, 2015. ISSN 0017-9310.

[7] H. F. Oztop and I. Dagtekin. Mixed convection in two-sided lid-driven differentially heated square cavity. *International Journal of Heat and Mass Transfer*, 47(8):1761 – 1769, 2004. ISSN 0017-9310.

[8] M. Sheikholeslami and A. J. Chamkha. Flow and convective heat transfer of a ferro-nanofluid in a double-sided lid-driven cavity with a wavy wall in the presence of a variable magnetic field. *An International Journal of Computation and Methodology*, 69:1186–1200, 2016.

[9] Y. S. Daniel, Z. A. Aziz, Z. Ismail, and F. Salah. Numerical study of entropy analysis for electrical unsteady natural magnetohydrodynamic flow of nanofluid and heat transfer. *Chinese Journal of Physics*, 55(5):1821 – 1848, 2017. ISSN 0577-9073.

[10] M. Sheikholeslami and H. B. Rokni. Effect of melting heat transfer on nanofluid flow in existence of magnetic field considering Buongiorno Model. *Chinese Journal of Physics*, 55(4):1115 – 1126, 2017. ISSN 0577-9073.

[11] A. D. Orazio, A. Karimipour, A. H. Nezhad, and E. Shirani. Lattice Boltzmann method with heat flux boundary condition applied to mixed convection in inclined lid driven cavity. *Meccanica*, 50:945–962, 2015.

[12] F. Selimefendigil and A. J. Chamkha. Magnetohydrodynamics mixed convection in a lid-driven cavity having a corrugated bottom wall and filled with a non-Newtonian power-law fluid under the influence of an inclined magnetic field. *Journal of Thermal Science and Engineering Applications*, 8(2):021–023, 2016.

[13] A. Karimipour, A. D. Orazio, and M. S. Shadloo. The effects of different nano particles of Al_2O_3 and Ag on the MHD nanofluid flow and heat transfer in a microchannel including slip velocity and temperature jump. *Physica E: Low-dimensional Systems and Nanostructures*, 86:146 – 153, 2017. ISSN 1386-9477.

[14] F. Selimefendigil and H. F. Oztop. Natural convection and entropy generation of nanofluid filled cavity having different shaped obstacles under the influence

of magnetic field and internal heat generation. *Journal of the Taiwan Institute of Chemical Engineers*, 56:42 – 56, 2015. ISSN 1876-1070.

[15] A. J. Chamkha. Hydromagnetic combined convection flow in a vertical lid-driven cavity with internal heat generation or absorption. *An International Journal of Computation and Methodology*, 41:529–546, 2002.

[16] S. Hussain, K. Mehmood, M. Sagheer, and A. Farooq. Entropy generation analysis of mixed convective flow in an inclined channel with cavity with Al_2O_3-water nanofluid in porous medium. *International Communications in Heat and Mass Transfer*, 89:198–210, 2017.

[17] Y. Varol, H. F. Oztop, and I. Pop. Natural convection in a diagonally divided square cavity filled with a porous medium. *International Journal of Thermal Sciences*, 48(1405 - 1415), 2009. ISSN 1290-0729.

[18] F. M. White. *Fluid Mechanics*. McGraw Hill, 7th edition, 2011.

[19] Y. A. Cengel and J. M. Cimbala. *Fluid Mechanics*. McGraw Hill, third edition, 2013.

[20] R. K. Bansal. *A Textbook of Fluid Mechanics*. Firewall Media, first edition, 2005.

[21] W. M. Rohsenow, J. R. Hartnett, and Y. I. Cho. *Handbook of Heat Transfer*. McGraw Hill, 3rd edition, 1998.

[22] R. Saidur, K. Y. Leong, and H. A. Mohammed. A review on applications and challenges of nanofluids. *Renewable and Sustainable Energy Reviews*, 15(3): 1646 – 1668, 2011. ISSN 1364-0321.

[23] D. A. Nield and A. Bejan. *Convection in Porous Media*. Springer, fifth edition, 2006.

[24] J. H. Freziger and M. Peric. *Computational Methods For Fluid Dynamics*. Springer, 3rd edition, 2002.

[25] J. Kunes. *Dimensionless Physical Quantities in Science and Engineering*. Elsevier, first edition, 2012.

[26] C. C. Cho, C. L. Chen, and C. K. Chen. Mixed convection heat transfer performance of water-based nanofluids in lid-driven cavity with wavy surfaces. *International Journal of Thermal Sciences*, 68:181 – 190, 2013. ISSN 1290-0729.

[27] L. K. Saha, K. M. Salah Uddin, and M. A. Taher. Effect of internal heat generation or absorption on MHD mixed convection flow in a lid driven cavity. *American Journal of Applied Mathematics*, 3:20–29, 2015. ISSN 2330-0043.

[28] Z. Boulahia, A. Wakif, and R. Sehaqui. Numerical study of mixed convection of the nanofluids in two-sided lid-driven square cavity with a pair of triangular heating cylinders. *Journal of Engineering*, pages 1–8, 2016.

[29] M. Sheikholeslami, R. Ellahi, M. Hassan, and S. Soleimani. A study of natural convection heat transfer in a nanofluid filled enclosure with elliptic inner cylinder. *International Journal of Numerical Methods for Heat & Fluid*, 24: 1906 – 1927, 2014.

[30] A. Malleswaran and S. Sivasankaran. A numerical simulation on MHD mixed convection in a lid-driven cavity with corner heaters. *Journal of Applied Fluid Mechanics*, 9(1):311–319, 2016. ISSN 1735-3572.

[31] M. A. Sheremet and I. Pop. Mixed convection in a lid-driven square cavity filled by a nanofluid: Buongiorno's mathematical model. *Applied Mathematics and Computation*, 266:792 – 808, 2015. ISSN 0096-3003.

[32] R. Iwatsu, J. M. Hyun, and K. Kuwahara. Mixed convection in a driven cavity with a stable vertical temperature gradient. *International Journal of Heat and Mass Transfer*, 36(6):1601 – 1608, 1993. ISSN 0017-9310.

[33] L. K. Saha, K. M. Salah Uddin, and M. A. Taher. Effect of internal heat generation or absorption on MHD mixed convection flow in a lid driven cavity.

International Journal of Heat and Mass Transfer, 3:20–29, 2015. ISSN 2330-0043.